THE KINEMATICS OF BREAKING WAVES IN THE SURF ZONE.

Alfred James Olsen

NAVAL POSTGRADUATE SCHOOL
Monterey, California

THESIS

THE KINEMATICS OF BREAKING WAVES

IN THE SURF ZONE

by

Alfred James Olsen

September 1977

Thesis Advisor: Edward B. Thornton

SECURITY CLASSIFICATION OF THIS PAGE (When Data Entered)

REPORT DOCUMENTATION PAGE

READ INSTRUCTIONS BEFORE COMPLETING FORM

1. REPORT NUMBER	2. GOVT ACCESSION NO. / 3. RECIPIENT'S CATALOG NUMBER
4. TITLE (and Subtitle): The Kinematics of Breaking Waves in the Surf Zone	5. TYPE OF REPORT & PERIOD COVERED: Master's Thesis; September 1977
	6. PERFORMING ORG. REPORT NUMBER
7. AUTHOR(s): Alfred James Olsen	8. CONTRACT OR GRANT NUMBER(s)
9. PERFORMING ORGANIZATION NAME AND ADDRESS: Naval Postgraduate School, Monterey, California 93940	10. PROGRAM ELEMENT, PROJECT, TASK AREA & WORK UNIT NUMBERS
11. CONTROLLING OFFICE NAME AND ADDRESS: Naval Postgraduate School, Monterey, California 93940	12. REPORT DATE: September 1977
	13. NUMBER OF PAGES: 77
14. MONITORING AGENCY NAME & ADDRESS (if different from Controlling Office): Naval Postgraduate School, Monterey, California 93940	15. SECURITY CLASS. (of this report): Unclassified
	15a. DECLASSIFICATION/DOWNGRADING SCHEDULE

16. DISTRIBUTION STATEMENT (of this Report)

Approved for public release; distibution unlimited

17. DISTRIBUTION STATEMENT (of the abstract entered in Block 20, if different from Report)

18. SUPPLEMENTARY NOTES

19. KEY WORDS (Continue on reverse side if necessary and identify by block number)

breaking waves
surf zone

20. ABSTRACT (Continue on reverse side if necessary and identify by block number)

Simultaneous measurements of sea surface elevation and onshore and alongshore water particle velocities were measured at three locations within the surf zone using two capacitance type penetrating wave staffs and three two-component electromagnetic flow meters. The probability density functions, pdf, for the sea surface elevation were always highly positively skewed, whereas the pdf's for the velocities were both negatively and positively skewed.

DD FORM 1 JAN 73 1473 EDITION OF 1 NOV 65 IS OBSOLETE
S/N 0102-014-6601

SECURITY CLASSIFICATION OF THIS PAGE (When Data Entered)

The Kinematics of Breaking Waves in the Surf Zone

by

Alfred James Olsen
Lieutenant, United States Navy
B.S., United States Naval Academy, 1972

Submitted in partial fulfillment of the
requirements for the degree of

MASTER OF SCIENCE IN OCEANOGRAPHY

from the

NAVAL POSTGRADUATE SCHOOL
September 1977

ABSTRACT

Simultaneous measurements of sea surface elevation and onshore and alongshore water particle velocities were measured at three locations within the surf zone using two capacitance type pentrating wave staffs and three two-component electromagnetic flow meters. The probability density functions, pdf, for the sea surface elevation were always highly positively skewed, whereas the pdf's for the velocities were both negatively and positively skewed. Mean values of the onshore and alongshore components of flow reflected the influence of a rip current frequently observed just south of the instrument locations. Strong harmonics in the spectra of sea surface fluctuations and particle velocities infer nonlinear conditions. Coherence values between waves and onshore flow were high, ranging above 0.9. The coherence between waves and onshore flow was used to separate the turbulence and wave-induced velocity components. Over the range of collapsing to spilling breakers a reasonable value for the ratio of turbulent to wave-induced velocity was determined to be approximately 0.75. Saturation regions were found in the wave and velocity energy-density spectra at higher frequencies as evidenced by -5 and -3 slopes, respectively.

TABLE OF CONTENTS

LIST OF TABLES

LIST OF FIGURES

ACKNOWLEDGEMENTS

I would like to express my deep appreciation to Dr. Edward B. Thornton for his understanding, knowledge and assistance without which this project would not even have started, much less reach fruition. I would also like to thank my wife, Dana, for her patience and typing. Of particular assistance was the Computer Center "night crew."

I. INTRODUCTION

A. HISTORICAL PERSPECTIVE

The surf zone is an area bounded on the seaward side by the point where waves first begin to break, and on the landward side by the point of maximum run-up on the beach slope. Although beach profiles and waves within the surf zone have been studied by many, the kinematics of wave forms and water particle velocities in the zone have remained something of a mystery.

The problems encountered have been practical as well as theoretical. Wave theories developed for deep water waves do not correctly characterize the motion which occurs as the waves break. Direct measurements of breaking waves appear to be the most viable means of approaching the problem. However, this has been hampered by the surf zone's hostile environment, which is difficult to reproduce in the laboratory, and by inadequate instrument design. Improvements in the latter area has resulted in sturdy, sensitive, but expensive measuring devices which have rapid response times.

The earliest study of significant importance was conducted by Iversen (1953) in which he used photographic techniques to obtain a Lagrangian description of water particle motion under breaking waves. The laboratory channel limited the wave type to plunging and surging breakers.

Inman (1956) was one of the first to make sophisticated field measurements, measuring the drag force on a cantilevered sphere to infer water particle motion. Miller and Zeigler (1964) measured in situ

particle motions using acoustic and electromagnetic current meters, then compared their findings with higher order wave theory and found some qualitative agreement. Walker (1969) made similar measurements using propeller type flow meters. Meadows (1976) used ducted impeller flow meters at equally spaced vertical positions in order to measure longshore components of flow. Huntley (1976) utilized a single two-component electromagnetic flow meter in an effort to obtain a value of the friction coefficient. Bowen and Huntley (1974) made measurements of the nearshore velocity fields using as many as three two-component electromagnetic flow meters. Führböter and Büsching (1974) measured simultaneous orbital velocities and water levels using a two-component current meter and two pressure type wave meters. Thornton (1969), Steer (1972), Thornton and Richardson (1973), Bub (1974) and Galvin (1975) used pressure meters, capacitace wave gauges and electromagnetic current meters to compute particle velocities and surface profiles within the surf zone. The work presented herein is an extension of these latter studies.

B. OBJECTIVE

The objective of this research is to study the kinematics of water particles within breaking waves and within the surf zone. In particular, the experiment was performed on a flat beach in order to measure the characteristics of spilling breakers. Simultaneous measurements were made of the instaneous sea surface elevation and two orthogonal water particle velocities, onshore and alongshore, at three fixed locations in the surf zone. Estimates of the probability density functions and

power spectra of the wave heights and particle velocities are made. The suitability of using linear wave theory as a spectral transfer function in determining velocity spectral components from the power spectrum of the waves is measured. Computed velocity spectra are compared with actually measured velocity spectra. Coherence between waves and onshore flow is used to separate the turbulence and wave-induced velocity components in order to determine the ratio of turbulent to wave-induced velocity. Spectral estimates are analyzed to ascertain the slope of the saturation region at higher frequencies.

II. MEASUREMENTS

A. EXPERIMENT

The experimental site is just north of La Jolla, California. Data presented in this study was taken as part of a larger scale experiment conducted from 15 February to 30 March 1977 in the Southern California bight area. The over-all purpose of the experiment was to test and evaluate the instrumentation package which was selected for use aboard SEASAT. The apparatus, which will measure waves, winds, and sea surface temperature, was being flown on board NASA airplanes. A major ground truth program was concurrently being conducted at Torrey Pines Beach.

Measurements of waves, currents, and sediment transport at Torrey Pines Beach were made using the following equipment. A five element linear array of pressure sensors was positioned offshore along the ten meter contour to measure wave energy and direction. Located in the surf zone inshore of the array were three support towers in a line perpendicular to the beach. A surface piercing capacitance wave gauge and a two-component electromagnetic flow meter were mounted on each tower. A nephelometer was installed on the middle support tower. To the north of the three towers was an array of four flow meters which was used to delineate the areal and temporal variation in alongshore currents. Figure 1 shows instrument locations. Resistance-wire run-up meters were installed in the swash zone at four locations. All instrumentation was battery operated.

The offshore pressure sensor outputs were telemetered directly to the shore processes lab at Scripps Institute of Oceanography, which is

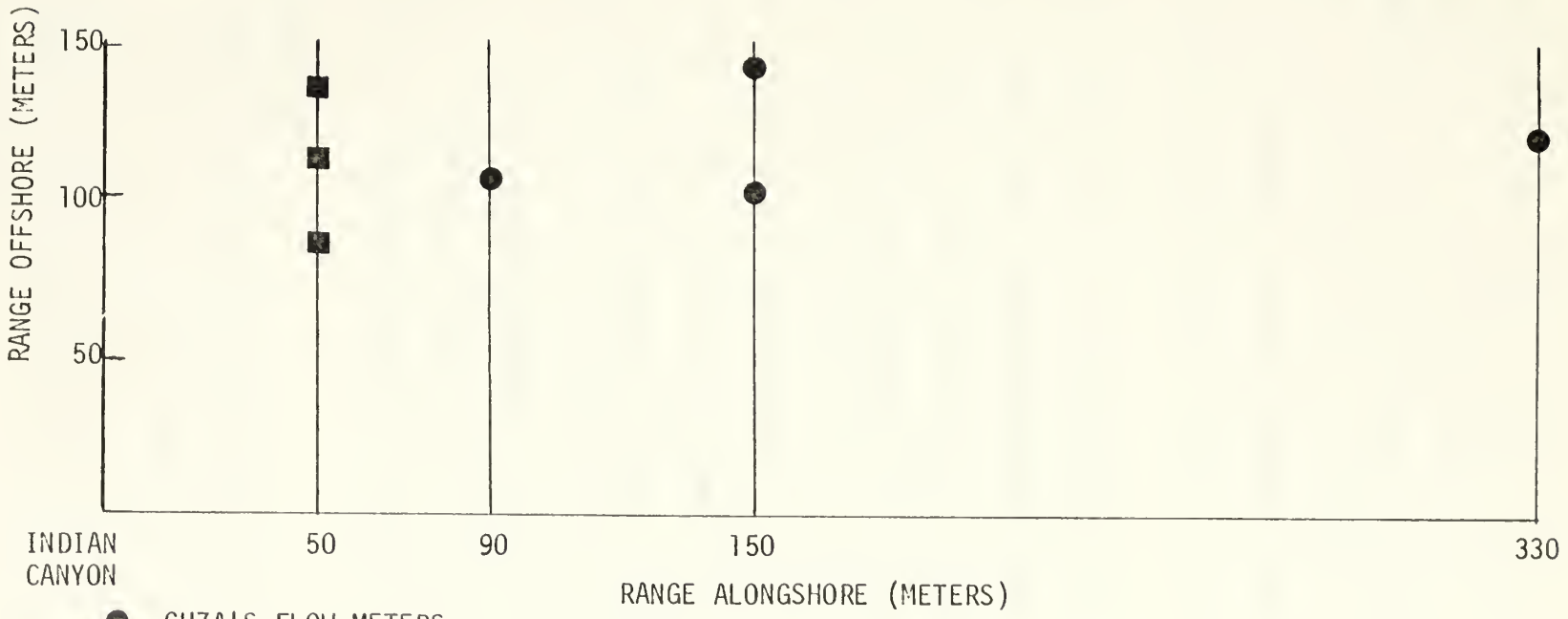

Figure 1. Instrument Location for Overall Experiment.

located one mile to the south. All data from the other instruments were cabled to one of two transmitting terminals on the beach where it was then telemetered to the shore processes lab and recorded. All the equipment except the nephelometer were in position prior to high tide on 9 March. The nepholometer was installed on 14 and 15 March. Data was accumulated during high tide on 9, 10, 11, 16, 17, 18, 19, 21 and 23 March.

Several other smaller scale experiments were conducted at the same time. At an elevation of approximately 300 feet on a cliff overlooking Torrey Pines Beach a radar installation was established. The radar images of waves were then photographed and analyzed.

Sediment transport experiments were conducted on 11, 21, and 23 March. Bed load transport was measured using the methods described by Inman and Komar (1970) to trace the movement of fluorescent dyed sand. Suspended sediments were measured in situ by swimmers using a mechanical water sampling devide. These samples were taken along with nepholometer readings in order to compare methods. During these sediment transport investigations, Lagrangian floats made from wine bottles weighted by sand were used to determine average long-shore current speeds.

B. INSTRUMENTATION.

The manner in which waves break depends very much on the characteristics of the beach and near shore bottom slope. (Table I) Spilling breakers occurred most frequently at the Torrey Pines Beach site. Figure 2 shows a typical beach profile and the location of the instruments which provided the data for this paper.

TABLE I. BEACH AND WAVE CHARACTERISTICS

LOCATION	TORREY PINES BEACH
DATE	9-23 MARCH 1977
BEACH SLOPE	FIGURE 2 and APPENDIX A
SAND TYPE	QUARTZ
SAND MEDIAN GRAIN SIZE	1.2 MILLIMETERS
BREAKER TYPE	SPILLING
WAVE PERIOD	11.9 to 15.9 SECONDS
WAVE HEIGHT	UP TO 1.5 METERS

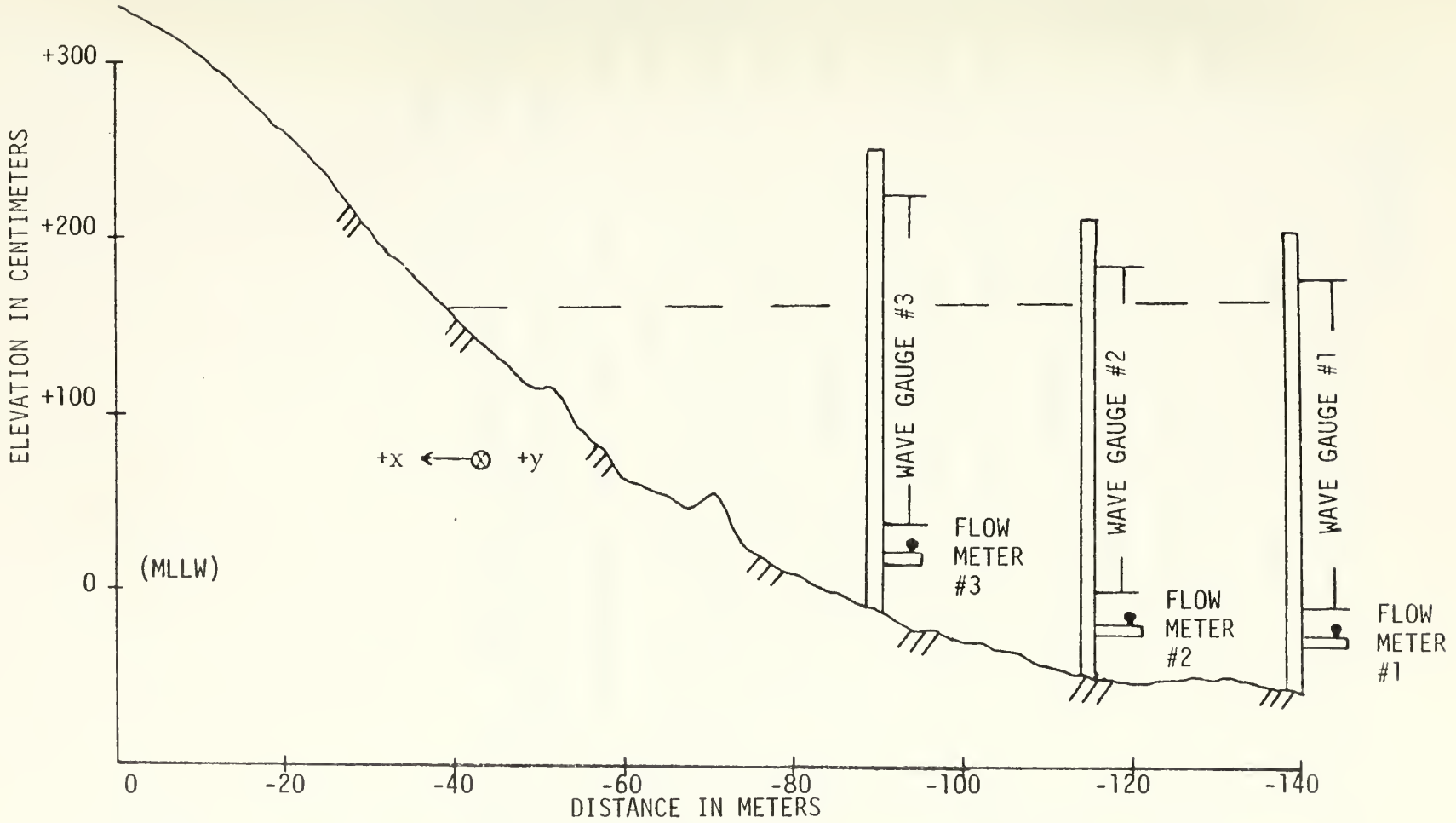

FIGURE 2. Typical Beach Profile and Instrument Location at Torrey Pines Beach on 19 March 1977

1. Wave Gauge

The wave gauges were of the capacitance type fashioned from 3/8 inch outside diameter stainless steel rod. The rod was tightly covered with 1/16 inch wall thickness polypropylene tubing. This linear, highly sensitive instrument has proven to be sufficiently sturdy to withstand the rigors of the unfriendly surf zone. The gauges operate on the principle that a change in the plate dimension of the capacitor changes its capacitance and consequently the circuitry output voltage. In these gauges, the insulated steel rod and sea water act as the plates and the insulation functions as the dielectric. As the water level fluctuated, the capacitance changed. Fluctuations were sensed by a transistorized circuit powered from the beach. The circuit was designed by McGoldrick (1969). The electronics packaged was housed in a watertight brass case which was mounted on the tower. This allowed the connecting leads to be relatively short, hence minimizing wire-to-wire capacitance. All gauges were statically calibrated in the laboratory prior to the experiment. Accuracy was estimated to be $\pm$.005m. The calibration plots are shown in Appendix B.

2. Flow Meter

The flow meters were Marsh-McBirney model 511 electromagnetic water current meters. Operation of the meter is based on Faraday's principle of electromagnetic induction. The meter measures water particle velocity in two orthogonal directions through a range of zero to three m/sec with a maximum output error of two percent of full scale reading. The sensor has a variable time constant, a setting of 0.2 sec. was used.

The flow meters were dynamically calibrated using the method of Thornton and Krapohl (1974). This procedure involves utilizing an oscillating platform driven by a variable speed motor geared to an eccentric throw arm. This technique was employed in order to determine the meter's characteristics. Measurement accuracy was determined to be $\pm$.005 m/sec. The only difficulty encountered in their utilization occurred when Flow Meter #1 was buried on 19 March due to the heavy sediment transport.

The measuring instruments were attached to a 3.6m high tower constructed of steel pipe with an outside diameter of 6.3cm.A 0.5m diameter base plate was placed about 0.6m from the bottom of the tower. This configuration allowed the tower to be sunk approximately 0.7m into the sand. The towers were also supported by steel guy wires fastened to blade anchors driven into the sand. Thus, tower movement and vibration were negligible.

The towers were placed on a line perpendicular to the shore at specified distances, and were erected during low tide when the beach was more accessible. As indicated earlier, measurements were taken at

high tide. Instruments were arranged so as to be in the same vertical plane. A carpenter's level was used to establish axis alignment with an estimated error of ± 2 degrees. A typical tower and instrument arrangement is shown in Figure 3.

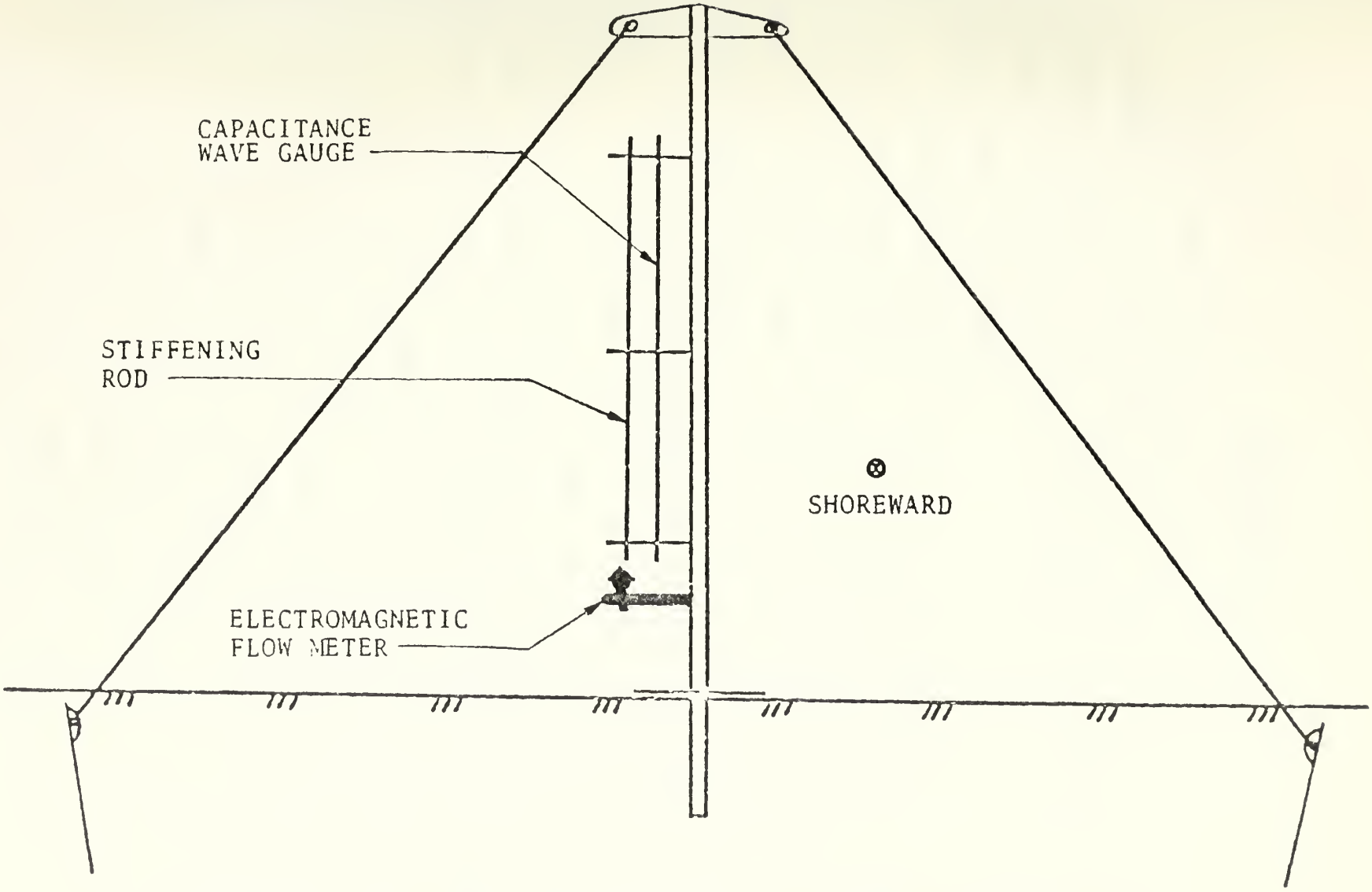

FIGURE 3. Schematic of Typical Instrument Tower with Sensors

III. ANALYSIS OF DATA

The data were digitized at a rate of four samples per second, corresponding to a sample interval of 0.25 seconds. This resulted in a Nyquist frequence of 2.0 Hz. The sampling rate was considered sufficiently high enough to avoid aliasing of energy into the portion of the spectra which was of interest.

Continuous time series records of all measurements were taken for roughly 2-1/2 hours each day. Record lengths of 24 minutes from each data set were subjected to analysis. Criteria which determined record lengths included economy of computer usage and resolution over the frequency range of interest.

A maximum lag time was chosen as 5% of the record length. This resulted in a spectral band width resolution of 0.007 Hz and each spectral estimate having 40 degrees of freedom. The ninety percent confidence limits for 40 degrees of freedom using a chi-square distribution are found to be between 0.72 and 1.51 of the measured power spectral estimates.

A mean value was computed for all data sets and the data was linearly detrended to remove tidal effects. Variance, standard deviation and average period were calculated. The average period was determined by calculating the time between zero upcrossings. The calculated average periods are lower than the visually observed periods due to a number of perturbations, such as noise and capillary waves, increasing the zero upcrossing occurrences. A probability density function for each data set was calculated and plotted. Comparisons were made with Gaussian and Gram-Charlier distributions using the chi-square goodness-of-fit test. Variance,

standard deviation, skewness and kurtosis of the distributions were computed and are summarized in Table II.

For each data set an auto-covariance function was determined and then smoothed with a Parzen window. Applying a Fourier transform to the smoothed auto-covariance function resulted in the power spectrum. An examination of the power spectrum shows the regions of greatest potential or kinetic energies and their respective frequencies.

Cross-spectra were computed by calculating a cross-covariance between data sets, smoothing it with a Parzen window and applying a Fourier transform. Coherence and phase were then determined from the cross-spectrum. A coherence and phase versus frequency plot will indicate the regions and degree of linear relationship and phase between two data sets.

TABLE II. COMPUTED STATISTICS

DATE	INSTRUMENT	MEAN	VARIANCE	STANDARD DEVIATION	SKEWNESS	KURTOSIS	CHI-SQUARE PARAMETER GAUSSIAN	CHI-SQUARE PARAMETER GRAM-CHARLIER
16 March	WG#1	0.88374	0.04535	0.21295	0.21731	2.57819	630.66	477.17
	FM#1							
	ONSHORE	-0.11879	0.21609	0.46485	0.18605	3.00899	113.15	82.57
	ALONGSHORE	-0.09757	0.04803	0.21917	-0.07339	3.61131	104.75	95.67
	FM#2							
	ONSHORE	0.28816	0.13883	0.37260	-0.44367	3.24272	742.04	528.98
	ALONGSHORE	0.01382	0.01883	0.13723	0.11371	3.61106	180.76	171.82
	FM#3							
	ONSHORE	-0.04116	0.19047	0.43643	0.15591	3.07524	89.69	64.67
	ALONGSHORE	0.58692	0.03909	0.19770	-0.13319	3.18835	116.02	85.16
	WG #3	-	-	-	-	-	-	-
17 March	WG#1	1.26267	0.06452	0.25401	1.32098	5.09639	5016.52	2515.77
	FM#1							
	ONSHORE	-0.40482	0.24035	0.49025	0.18816	3.09840	141.70	171.50
	ALONGSHORE	0.26711	0.04676	0.21625	-0.07613	3.55094	90.61	102.65
	FM#2							
	ONSHORE	0.22352	0.18673	0.43212	-0.08117	3.44394	219.86	191.98
	ALONGSHORE	1.12691	0.03998	0.19995	-0.02864	3.04642	154.48	153.67
	FM#3							
	ONSHORE	-0.11419	0.28388	0.53281	0.14974	2.77769	123.54	101.96
	ALONGSHORE	-0.11369	0.04181	0.20448	-0.25591	3.44876	524.35	427.73
	WG#3	-	-	-	-	-	-	-
18 March	WG #1	1.32682	0.04614	0.21480	1.64765	6.52515	5724.65	2321.19
	FM #1							
	ONSHORE	-0.94626	0.33726	0.58074	0.28457	3.16107	123.98	68.02
	ALONGSHORE	0.49211	0.06977	0.26414	0.22253	4.85216	234.98	127.10
	FM #2							
	ONSHORE	0.34363	0.16916	0.41129	-0.12491	2.98118	113.38	130.31
	ALONGSHORE	0.70356	0.03569	0.18892	0.05421	2.90916	63.10	60.42
	FM #3							
	ONSHORE	-0.11006	0.22473	0.47406	0.04931	3.14917	111.19	119.53
	ALONGSHORE	0.22176	0.04266	0.20653	-0.18522	3.77259	81.61	98.96
	WG #3		0.02006	0.14164	0.25536	4.14267	926.14	1011.97

TABLE II. COMPUTED STATISTICS (Continued)

DATE	INSTRUMENT	MEAN	VARIANCE	STANDARD DEVIATION	SKEWNESS	KURTOSIS	CHI-SQUARE PARAMETER GAUSSIAN	CHI-SQUARE PARAMETER GRAM-CHARLIER
19 March	WG#1	1.25410	0.03791	0.19472	1.15469	5.92272	2524.97	1431.11
	FM#1							
	ONSHORE	0.25471	0.03847	0.19613	0.16774	3.03523	128.62	111.19
	ALONGSHORE	0.02497	0.15569	0.39458	-0.22020	3.18962	75.98	119.18
	FM#2							
	ONSHORE	-0.57159	0.27930	0.52849	-0.30074	2.80925	189.07	97.44
	ALONGSHORE	0.36404	0.07720	0.27785	0.20495	2.98625	110.01	61.12
	FM#3							
	ONSHORE	-0.32469	0.06231	0.24962	-0.58402	5.23765	265.08	185.66
	ALONGSHORE	-1.19162	0.28912	0.53770	0.34196	3.18185	218.52	89.63
	WG#3		0.02629	0.16215	0.11407	2.69216	473.86	437.47
21 March	WG #1	0.97717	0.03958	0.19895	0.41770	3.18017	642.77	527.66
	FM #1							
	ONSHORE	-0.14119	0.20242	0.44922	0.02249	5.22612	284.28	611.77
	ALONGSHORE	-	-	-	-	-	-	-
	FM #2							
	ONSHORE	0.28811	0.22239	0.47158	-0.27077	3.21421	318.33	250.37
	ALONGSHORE	0.42430	0.03834	0.19580	0.58273	8.28218	162.60	55545.86
	FM #3							
	ONSHORE	0.07803	0.12168	0.34883	0.19327	3.67616	351.79	276.62
	ALONGSHORE	0.56900	0.03207	0.17909	0.18953	3.13666	131.71	90.40
	WG #3	0.83354	0.02314	0.15211	0.97536	3.89613	1252.74	282.93
23 March	WG #1	0.66638	0.04283	0.20694	0.95524	3.43183	1502.65	608.98
	FM #1							
	ONSHORE	-0.18851	0.21596	0.46471	0.61468	4.01892	114.37	307.68
	ALONGSHORE	-	-	-	-	-	-	-
	FM #2							
	ONSHORE	0.24429	0.17855	0.42256	-0.35846	2.92472	237.72	112.23
	ALONGSHORE	0.09471	0.02642	0.16256	0.42730	3.70857	202.88	57.19
	FM#3							
	ONSHORE	0.03293	0.10178	0.31903	-0.50811	6.00248	300.28	1470.93
	ALONGSHORE	0.68297	0.02817	0.16783	-0.21501	3.46931	79.09	75.38
	WG #3	0.53540	0.00815	0.09030	1.20997	4.34993	3788.28	1634.04

Mean and variance for the wave heights is given in meters squared; mean and variance for the velocity components is given in meters squared per second squared.

Standard deviation for the wave heights is given in meters; standard deviation for the velocity components is given in meters per second.

IV. RESULTS

A. QUALITATIVE DESCRIPTION

Observation of various breaker types which occur on different beaches has resulted in a number of similarities being noted. A typical analog record of waves and onshore velocities obtained at Torrey Pines Beach is shown in Figure 4. In general, a sawtooth shaped profile is created when there is a quick drawdown of water just before the breaker arrives, followed by a steep, vertical leading edge, and a sloping profile toward the trailing edge. On the trailing edge, secondary waves are often observed. Secondary waves are harmonics of the primary wave frequency and denote strongly nonlinear waves. At Torrey Pines Beach the breaking waves are generally of the spilling variety which spill rapidly at the crest and move down the wave.

B. MEAN VALUES

A mean value was computed for all data sets and linearly detrended to remove tidal effects. The sea surface elevation mean values ranged from 0.67 to 1.33. Wave heights increased till the 18th and then decreased during the remaining period data was taken, reflecting well the actual environment.

Analysis of the mean values for both the onshore and alongshore components of flow was complicated by an apparent rip current. A rip current was frequently observed located just south of the array of wave gauges and flow meters. The on-offshore flow for the five days under consideration at Flow Meter #1 was always directed offshore at about 0.1

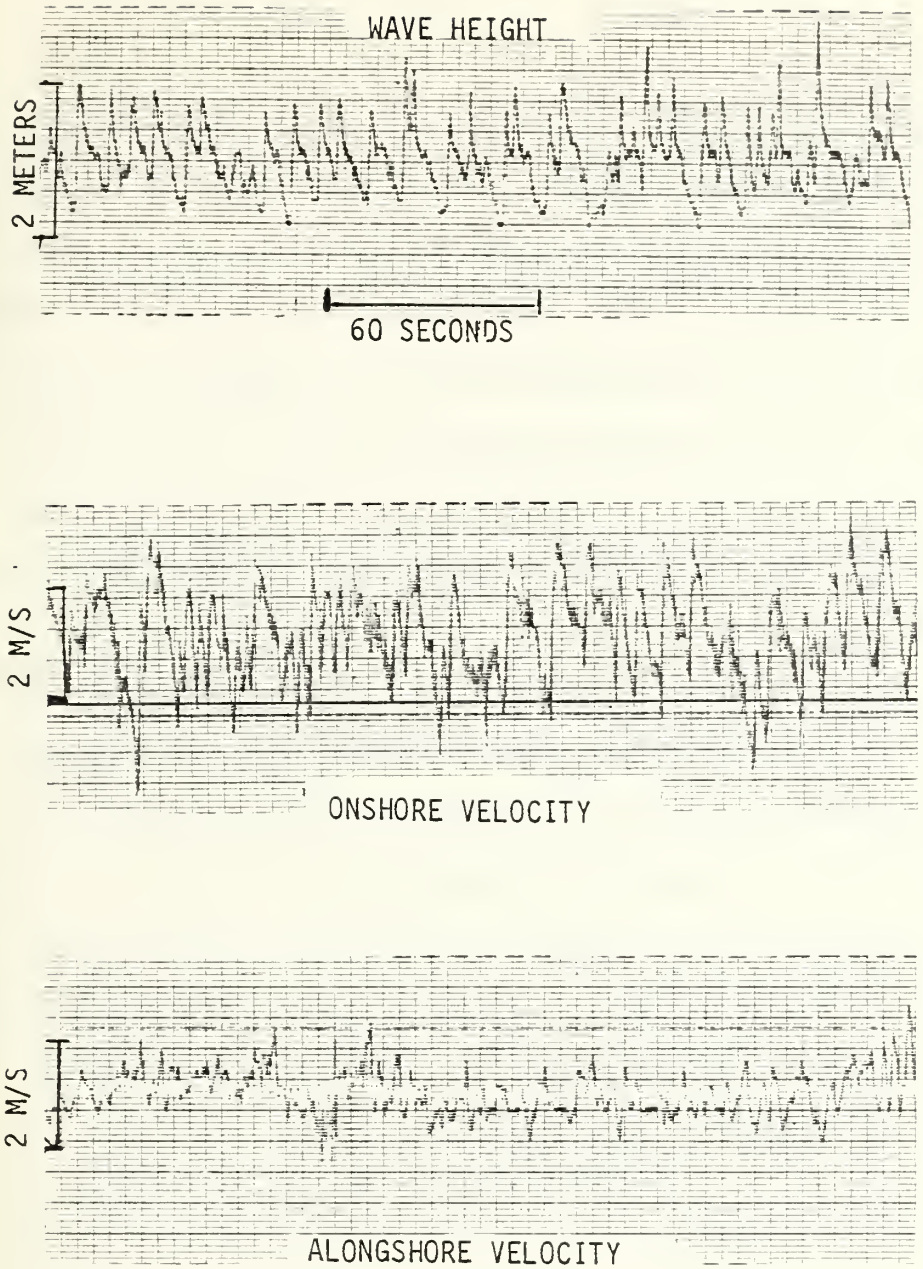

Figure 4. Typical Analog Record of Waves and Velocities from Torrey Pines Beach.

m/sec. At Flow Meter #2 the horizontal water particle velocity was directed onshore at roughly 0.25 m/sec. The flow at Flow Meter #3 was away from the coast on 16, 17, and 18 March at slow speeds and towards the shore on 21 and 23 March moving very slowly. Concurrently, the longshore flow at Flow Meters #1, #2 and #3 was generally moving downcoast with the peak velocity varying from flow meter to flow meter from day to day. Similar results were reported by Huntley and Bowen (1974) for a nearshore circulation cell which they attributed to a rip current.

C. PROBABILITY DENSITY FUNCTIONS

1. Gaussian and Gram-Charlier Frequency Distributions

The computed probability density function was compared to the Gaussian and Gram-Charlier distributions and tested for comparison using the chi-square goodness-of-fit test. The closer the chi-square fit parameter is to zero, the better the fit (Table II).

The Gaussian probability density function is given by

$$P_{Ga}(x) = \frac{1}{\sigma \sqrt{2\pi}} e^{-(x-\mu)^2/2\sigma^2} \qquad (1)$$

where σ is the standard deviation and μ is the mean. The Gaussian distribution is completely described by the mean and variance, and has zero skewness and a kurtosis equal to three. This approximates the sea surface in deep water conditions. However, nonlinearities found in the surf zone introduce skewness and kurtosis values that deviate from Gaussian and result in a distribution more closely approximated by the

Gram-Charlier distribution. This is to be expected in that the Gram-Charlier pdf is calculated using the assigned parameters from the data, and includes moments higher than the second. The frequency distribution of Wave Gauge #1 on 23 March is shown in Figure 5. Appendix D contains distributions calculated for other data sets.

Distributions for all flow velocities are either unimodal or have less pronounced secondary peaks compared to the distributions of wave heights. The distribution of the onshore flow of Flow Meter #1 on 23 March is shown in Figure 6. As noted in Table II, this results in nearly equal fit parameters with the Gram-Charlier distribution being generally smaller and thus a better fit. Fit parameters for velocity components are much closer to zero than are the values calculated for wave components since the flow meters do not experience the surface irregularities to the same degree as do the wave gauges.

2. Skewness and Kurtosis

The sea surface distribution was found to be positively skewed. This means that positive values are large, but less frequent than negative values which are more frequent, but smaller, indicating a greater amount of time below the mean water level. In other words, the crests are steeper and more peaked, whereas the troughs are elongated and flatter which is how waves in shallow water theoretically appear.

It should follow that the wave-induced particle velocities would have distribution similar to the waves. However, of the 34 cases listed in Table II, 17 had positive skewness and 17 had negative skewness with no readily apparent pattern. Skewness of the onshore flow at Flow Meter #1

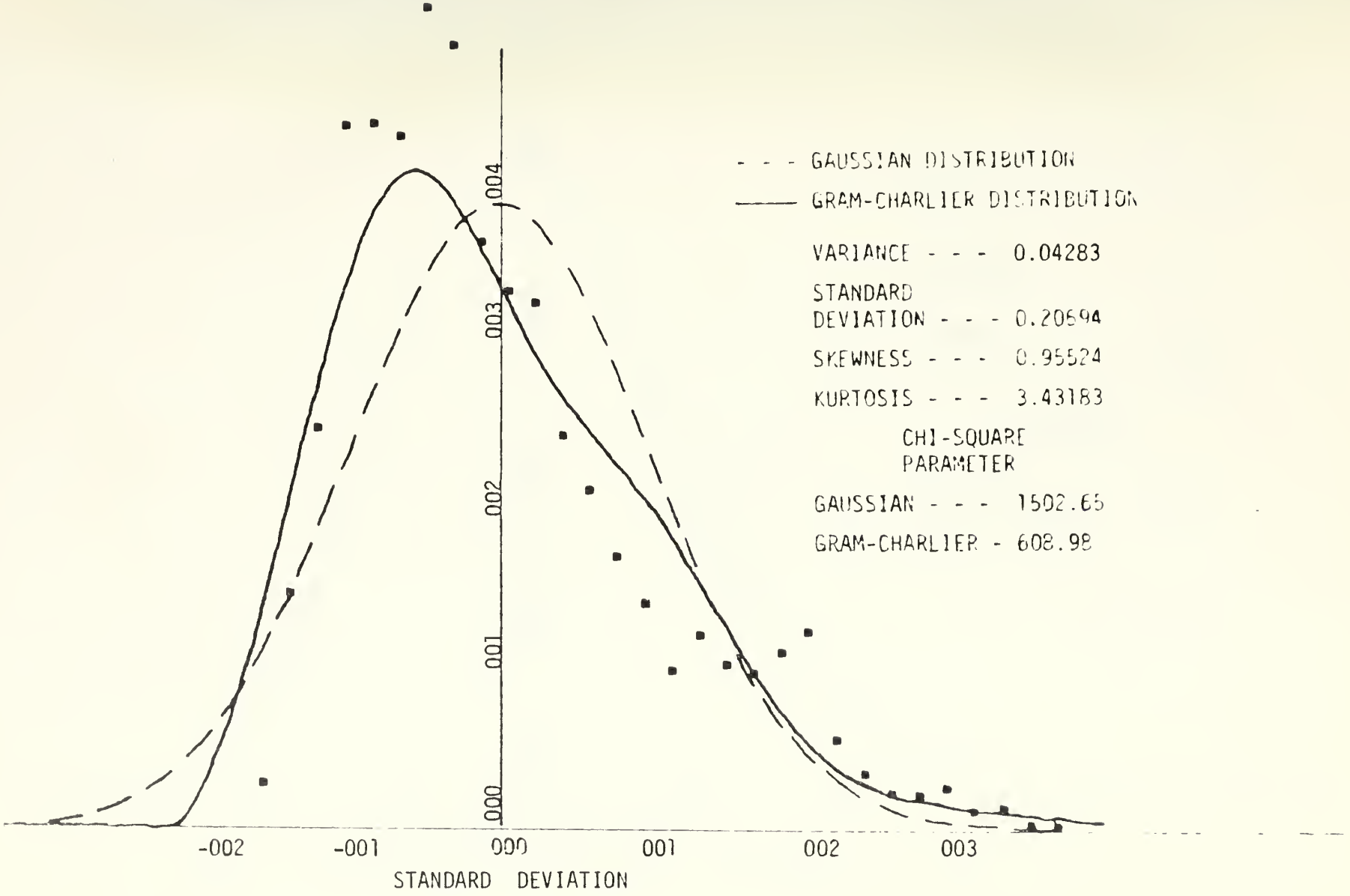

Figure 5. Frequency Distribution of the Sea Surface Elevation at Wave Gauge #1 on 23 March 1977.

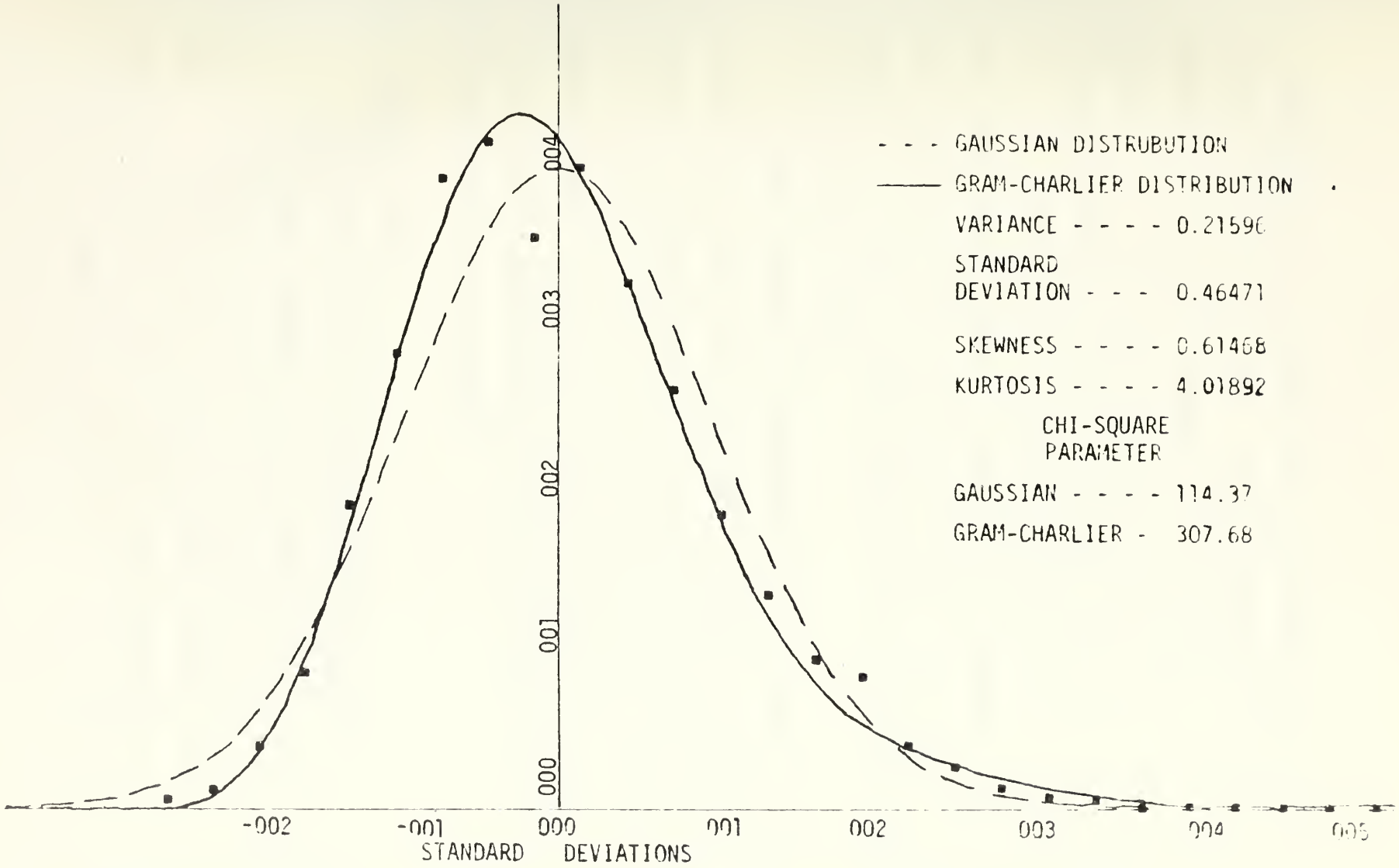

Figure 6. Frequency Distribution of the onshore flow at Flow Meter #1 on 23 March 1977.

was always positive. Alongshore flow at the same location had negative skewness in three of four cases. Onshore water particle velocity at Flow Meter #2 had negative skewness for all six days. The skewness of alongshore flow at the same point was positive in five of six cases. The onshore component of flow at Flow Meter #3 had a positive skewness for 16, 17, and 18 March and a negative skewness for the following three days on which data was taken. Skewness of the alongshore flow at Flow Meter #3 was positive for four of the six days. The reason for this disparity is not known. Similar anomalous results have been found by Thornton and Galvin (1975).

Kurtosis indicates the peakedness of each parameter. Just prior to breaking the waves achieve the greatest degrees of peakedness. Visual observations indicated that most of the waves were breaking at or near Wave Gauge #1 on 17, 18, and 19 March; this correlates with their high kurtosis values on these days. Values of kurtosis for all flow velocities again had no apparent pattern with values ranging from 2.6 to 8.6. The reason for this is not known.

D. SPECTRAL ANALYSIS

1. Sea Surface Elevation and Water Particle Velocity

The power, coherence, and phase spectra of Wave Gauge #1 and the onshore component of the flow of Flow Meter #1 on 23 March are shown in Figure 7. The spectrum of the wave surface elevation, which is characteristic of all the records, show a narrow banded peak at a frequency of 0.07 Hz, corresponding to a period of 14.3 sec. Also evident are

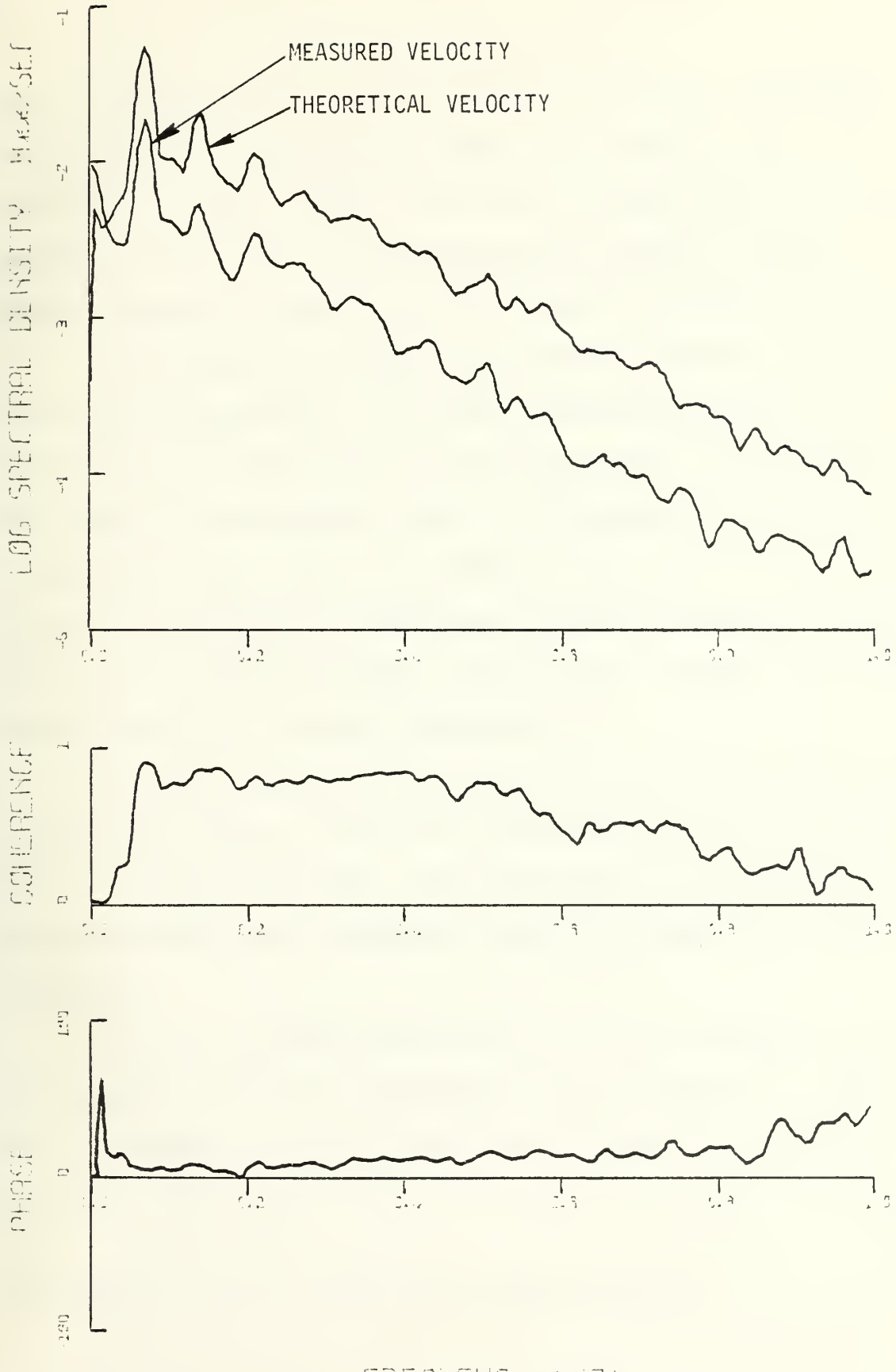

Figure 7. Power, Coherence and Phase Spectra for the onshore flow of Flow Meter #1 and Wave Gauge #1 on 23 March

peaks at 0.14 and 0.21 Hz which appear to be harmonics of the primary peak at 0.07 Hz. These harmonics appear to be physical as was observed from the strip chart earlier. The harmonics probably have some energy contribution due to the Fourier computational technique. Appendix E contains spectra calculated for all other wave and onshore flow data sets.

The coherence values were high, ranging to greater than 0.9 in the maximum energy portion of the wave. Coherence begins to fall off at about 0.5 Hz except on the 17th and 18th of March, the two days on which short-crested waves were noted. On these days the coherence begins to decrease at about 0.3 Hz. The decrease in coherence is probably due to the relative increase in turbulence, the general decrease in energy level, and wave energy spreading. The decrease in coherence due to wave energy spreading is discussed in Section E.

The phase angle, which according to linear theory should be zero, had an average value of less than 20 degrees over the highly coherent band of prominent wave energy. The phase angle tends to increase slightly over the coherent band and becomes random for the noncoherent region of the spectrum.

In order to compare waves and flow velocity, the wave profile spectrum was converted to a theoretical velocity spectrum for comparison with the measured flow velocity spectrum using the linear transfer function such that

$$S_U(f) = |H(f)|^2 S_\eta(f) \qquad (2)$$

The transfer function is given from linear wave theory

$$H(f) = 2\pi f \frac{\cosh k(h+z)}{\sinh kh} \qquad (3)$$

where

k is the wave number,

h is the mean water depth, and

z is the depth of flow meter below the mean depth (m)

Quantitatively, the results showed that linear theory overestimated wave-induced velocity spectral components by about 50%; in previous studies by Thornton et al (1976) where the waves were long crested and arrived at near normal incidence, the opposite was true, in that linear theory underestimated the magnitude of the wave spectrum. The difference in results is probably due to wave directionality, since when the wave approaches at any angle other than normal the flow meter measures only a component of the actual flow.

2. Onshore and Alongshore Flow

The cross-spectra between the onshore and alongshore components of flow were calculated with the intent of finding the relation between these two parameters. Power, coherence, and phase spectra of the onshore and alongshore flows at Flow Meter #3 on 23 March are shown in Figure 8. The spectra, which are representative of all the records, shows very little coherence between velocity components. The phase angle is random over the noncoherent band.

The reason for the lack of coherence between the two orthogonal flow components is believed to be due to wave directionality. As was seen earlier the onshore component of flow appears highly wave-induced;

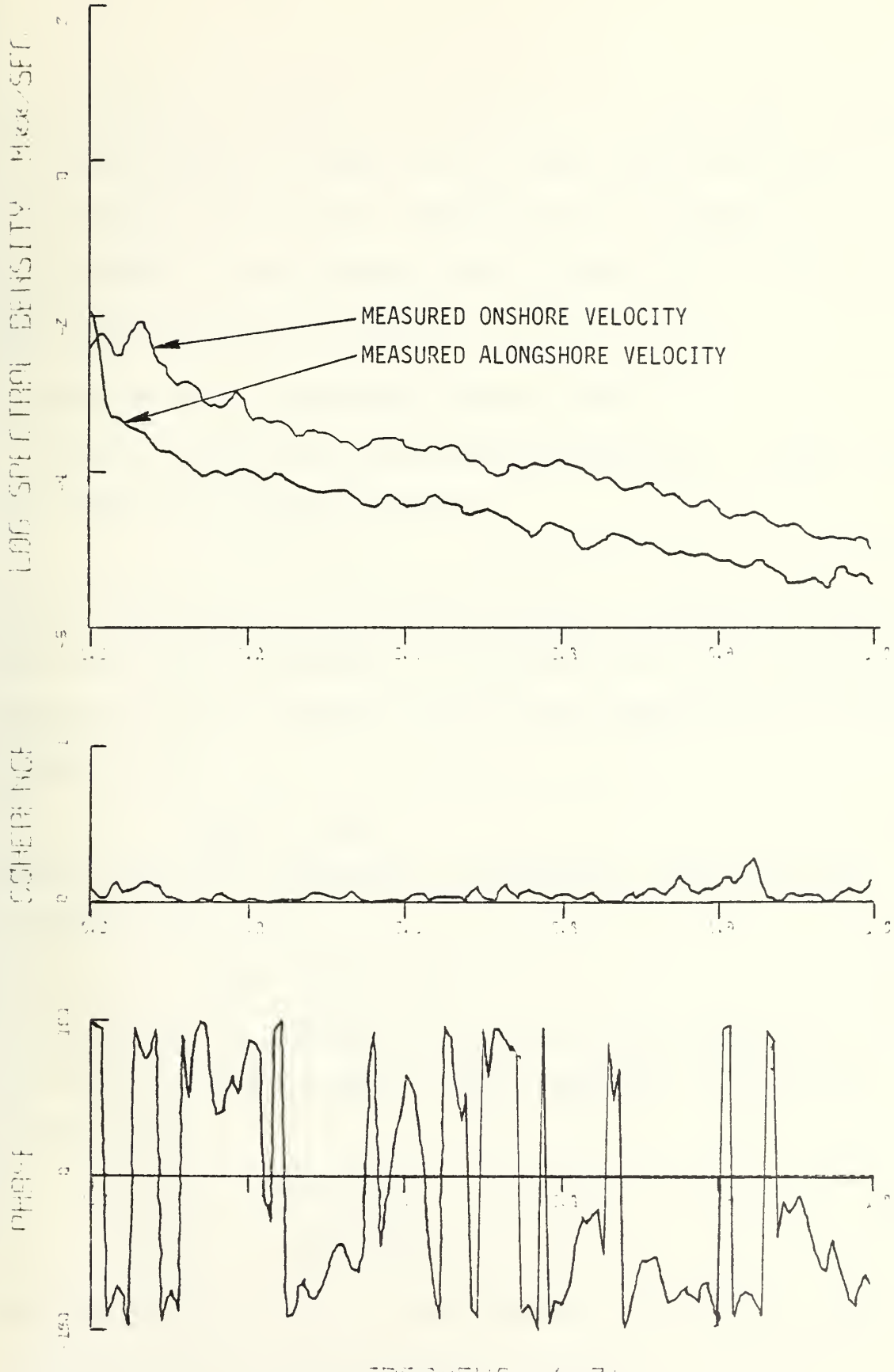

Figure 8 Power, Coherence and Phase Spectra for onshore and alongshore flow at Flow Meter #3 on 23 March.

concomitantly, the alongshore flow component is at near normal incidence to the wave direction and thus has only a small wave-induced contribution. The variance of the alongshore component of flow is significantly less than the on-offshore component except at zero frequency, which reflects the mean longshore current variation.

E. TURBULENT VELOCITY VERSUS WAVE-INDUCED VELOCITY

The total velocity can be separated into components of a mean, plus wave-induced, plus turbulent velocity

$$u = \bar{u} + U + u'. \tag{4}$$

The wave-induced and turbulent velocity spectral components are assumed to be statistically independent. For unidirectional waves aligned with the measured velocity component, the co-spectra between waves and velocity is then given by

$$S_{u\eta}(f) = S_{U\eta}(f). \tag{5}$$

Assuming statistical independence, the horizontal velocity spectrum is obtained from

$$S_u(f) = S_{u'}(f) + S_U(f). \tag{6}$$

A further assumption is made that the waves and wave-induced velocities are given by a constant parameter linear process where the coherence is equal to unity

$$\gamma^2_{U\eta}(f) = \frac{\left|S_{U\eta}(f)\right|^2}{S_U(f)S_\eta(f)} = 1. \tag{7}$$

Substituting (5), (6), and (7) into the definition of coherence between the total horizontal velocity and waves results in

$$\gamma^2_{u\eta}(f) = \left[1 + \frac{S_{u'}(f)}{S_U(f)} \right]^{-1} = \frac{S_U(f)}{S_u(f)} . \qquad (8)$$

Increasing lack of coherence is due to an increasing high ratio of turbulence. The coherence values indicate the percent of total velocity which is associated with the wave velocity.

Wave-induced velocity can be determined using (8)

$$S_U(f) = \gamma^2_{u\eta}(f) S_u(f). \qquad (9)$$

The wave-induced velocity spectral component calculated in this way should be less than the actual value, the reason for this being that the linear coherence between waves and velocities will always be underpredicted due to nonlinearities which are always large in a breaking wave and also as a result of directional spreading of the incident wave energy (Battjes (1974)).

The turbulent velocity spectrum is derived by subtracting the calculated velocity spectrum from the measured velocity spectrum,

$$S_{u'}(f) = S_u(f) - S_U(f). \qquad (10)$$

The ratio of the turbulent velocity intensity to the wave-induced velocities intensity is shown in Figure 9. The data used for collapsing and plunging breakers, denoted by squares, was measured during earlier studies by Thornton et al (1976). The collapsing and plunging breakers were measured on beaches where the waves were long crested and arrived at near normal incidence. The stars represent data collected during this experiment. A value of the velocity intensity is given by taking the

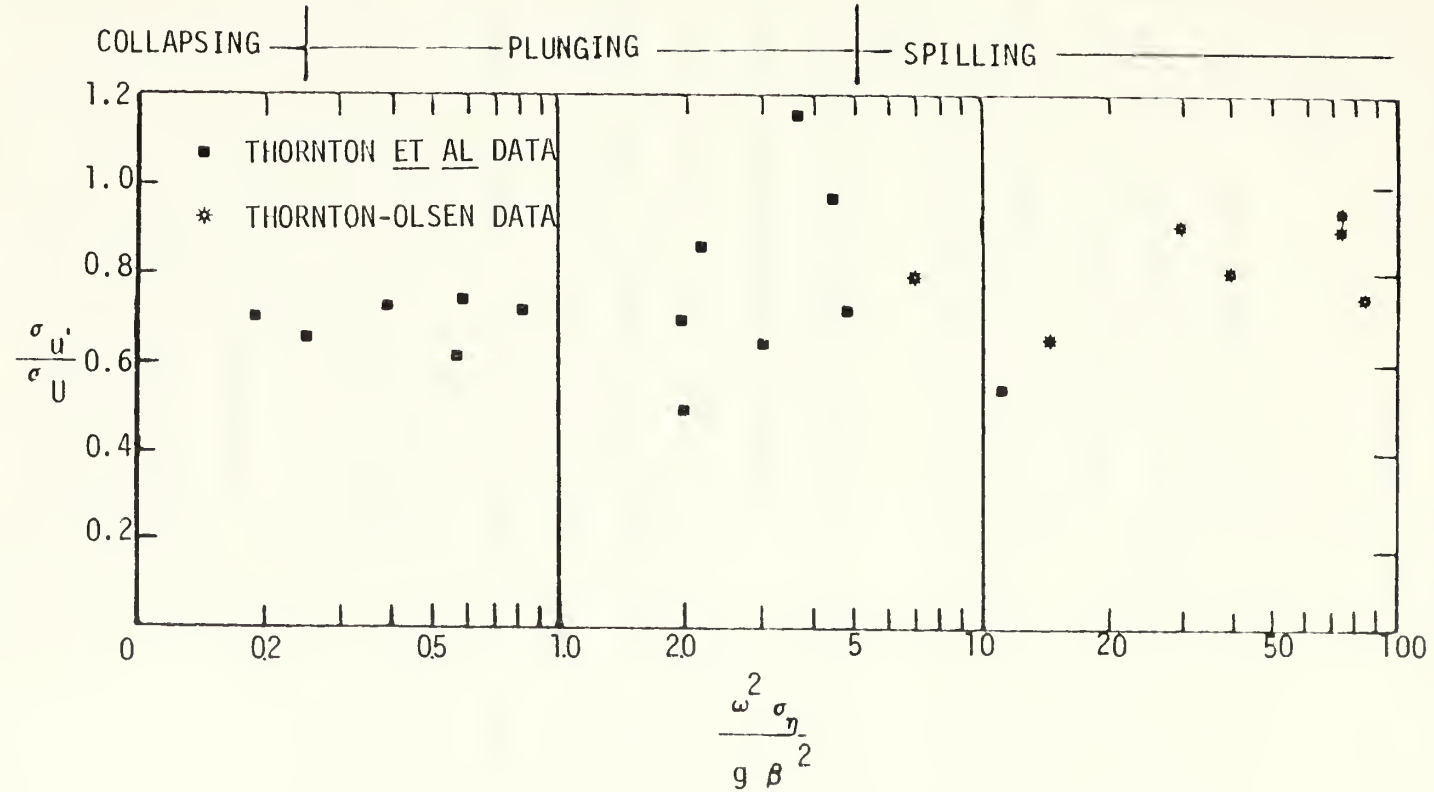

Figure 9. Ratio of turbulent to wave-induced velocity intensities

square root of the variance which is computed by integrating the velocity spectrum, $S_u(f)$, across all frequency bands

$$\sigma_u^2 = \int_0^\infty S_u(f)df. \tag{11}$$

The measurements show a small spread of values for the ratio of turbulent to wave-induced velocity intensities. The average ratio calculated is approximately 0.82. This would indicate that, to a first approximation, the wave-induced kinetic energy is approximately 1.2 times the turbulent kinetic energy. Thus the velocities in the surf zone on the average are highly wave-induced.

If waves are not unidirectional, and generally they are not, it is necessary to account for directional spreading. The wave angle striking the wave staff and the type of wave, long or short crested, must be considered. In general, short crested waves predominated at Torrey Pines Beach. On the 17th and 18th of March they were particularly noticeable. The coherence between surface elevation and velocity components of short crested waves is less than that of long crested waves due to directional spreading. Using the wave train model developed by Yefimov and Khristoforov (1971) the ratio of coherence between waves and onshore flow for the short crested waves to that for long crested waves is given by

$$\frac{\gamma^2_{u\eta}(f,\theta_s)}{\gamma^2_{u\eta}(f,\theta_1)} = \frac{(1 + 1/3\mathrm{ctn}^2\theta_o + 4S_{u'}(f)/3S_U(f))^{-1}}{(1 + S_{u'}(f)/S_U(f)[1/\cos^2\theta_o])^{-1}}. \tag{12}$$

The model describes long crested waves using a train of two-dimensional, planar random waves traveling in direction θ_o. This corresponds to a bivariate spectrum given by

$$\psi_\eta (f,\theta_1) = S_\eta(f)\delta(\theta-\theta_\circ) \quad , \tag{13}$$

where $\delta(\theta-\theta_\circ)$ is the Dirac delta function.

Short crested waves appear as a train of three-dimensional waves whose average direction of spectral components is assumed to be of the form

$$\psi_\eta (f,\theta_s) = \begin{cases} (2/\pi)\, S_\eta(f)\, \cos^2(\theta-\theta_\circ) \, , \\ 0 \quad \text{for} \mid \theta - \theta_\circ \mid > \pi/2 \, , \end{cases} \tag{14}$$

Neglecting turbulence in order to examine the effect of directionality, the ratio of the coherence between waves and wave-induced velocities for short crested waves to that of long crested waves becomes

$$\frac{\gamma^2_{U\eta}(f,\theta_s)}{\gamma^2_{U\eta}(f,\theta_1)} = \frac{(1 + 1/3\mathrm{ctn}^2\theta_\circ)^{-1}}{1} \, . \tag{15}$$

As an example, when $\theta_\circ$ equals an angle of 30°, the ratio equals 0.9.

Conversely, the influence of turbulence on the ratio of coherence between waves and velocities for short crested waves to that of long crested waves can be examined by disregarding the directionality and letting $\theta_\circ$=0. The ratio is given by

$$\frac{\gamma^2_{u\eta}(f,\theta_s)}{\gamma^2_{u\eta}(f,\theta_1)} = \frac{(\, 1 + 4S_{u'}(f)/3S_U(f) \,)^{-1}}{(\, 1 + S_{u'}(f)/S_U(f) \,)^{-1}} \, . \tag{16}$$

A summary of the ratios considering the turbulence and/or directionality factors at various angles is tabulated in Table III. The turbulence factor, $S_{u'}(f)/S_U(f)$, is assumed for comparison purposes to be equal to 0.75, the average value for the measured data in Figure 9 as denoted by the squares.

Table III

θ	$\gamma^2_{U\eta}(f,\theta_s)/\gamma^2_{U\eta}(f_1)$	$\gamma^2_{u\eta}(f_s)/\gamma^2_{u\eta}(f_1)$	$\gamma^2_{u\eta}(f,\theta_s)/\gamma^2_{u\eta}(f,\theta_1)$
	(Equation 15)	(Equation 16)	(Equation 12)
0		0.875	0.875
5	0.997		0.877
10	0.990		0.882
15	0.977		0.891
20	0.957		0.905
25	0.932		0.923
30	0.9		0.947

The coherence between waves and velocities was used to calculate the wave-induced velocity (equation 11). This method under-predicts the actual wave-induced velocity because of nonlinearities and wave energy spreading. Since the turbulent velocity is computed by subtracting the calculated wave-induced velocity spectrum from the measured velocity spectrum (equation 12) the smaller wave-induced velocity value makes the turbulent velocity value larger. The average ratio of the turbulent velocity intensity to the wave-induced velocity intensity was calculated to be 0.825. In order to correct for the directional spreading it is necessary to multiply by the ratio $\gamma^2_{u\eta}(f,\theta_s)/\gamma^2_{u\eta}(f,\theta_1)$. As an example, the ratio of the coherences for an angle of 15° is equal to 0.891. Multiplying this value by the average ratio results in a turbulence to wave-induced ratio of 0.75, which is equal to the earlier measured mean value. Hence

over the range of collapsing to spilling breakers a reasonable value for σ_u' / σ_U is approximately 0.75.

F. SATURATION REGION IN THE SPECTRUM OF BREAKING WAVES

Waves on Torrey Pines Beach characteristically broke as spilling breakers with the crest sliding down the face of the wave. When the fluid particles at the free surface move forward at a greater speed than the wave speed, c, breaking occurs. Strong harmonics observed in the wave and velocity spectra (Figure 7) are indicative of energy being transferred from low to higher frequencies. The energy is eventually dissipated by viscosity at the highest frequencies. When the transfer of energy is not rapid enough to balance the increase in energy density of the waves during shoaling, breaking occurs. The waves are said to be "saturated" with energy. Hence, a region of saturation would be expected through which energy is transferred from the low to higher frequencies. During shoaling and breaking of waves on a beach, the waves become saturated at low frequencies first imposing a bound on the peak energy density.

Spectra of waves at breaking, or just inshore of breaking, are shown in Figures 10 and 11 plotted on a log-log scale. The spectral estimates have been normalized by dividing by the total variance in an effort to bring the high end of the spectra to a single line. The spectral estimates have been block-averaged over frequency bands such that the log-energy values are linearly distributed on the log-frequency axis. The confidence intervals decrease with increasing frequency because of the increasing number of frequency bands averaged over. The

confidence interval is noted on the figures. The slopes of the log-log spectra at high frequencies for Wave Gauges #1 and Wave Gauges #3 can be approximated by a -5 slope. This is indicative of a saturation or equilibrium region for wind generated waves in deep water. This was a surprise, as a -3 slope was expected for the waves measured in shallow water, Thornton (1976). A possible explanation is that most of the waves measured were waves inside the initial break point and would be classified as spilling breakers or reformed waves. It may be that these types of waves do not reach saturation condition as found for the more intense plunging and collapsing breakers.

The normalized velocity spectra are given in Figures 12 and 13. The slopes of the velocity spectra at higher frequencies at Flow Meter #1 and Flow Meter #3 are both closely approximated by a -3 slope. A -3 slope is expected for the equilibrium region in both deep and shallow water and is consistent with the wave slopes.

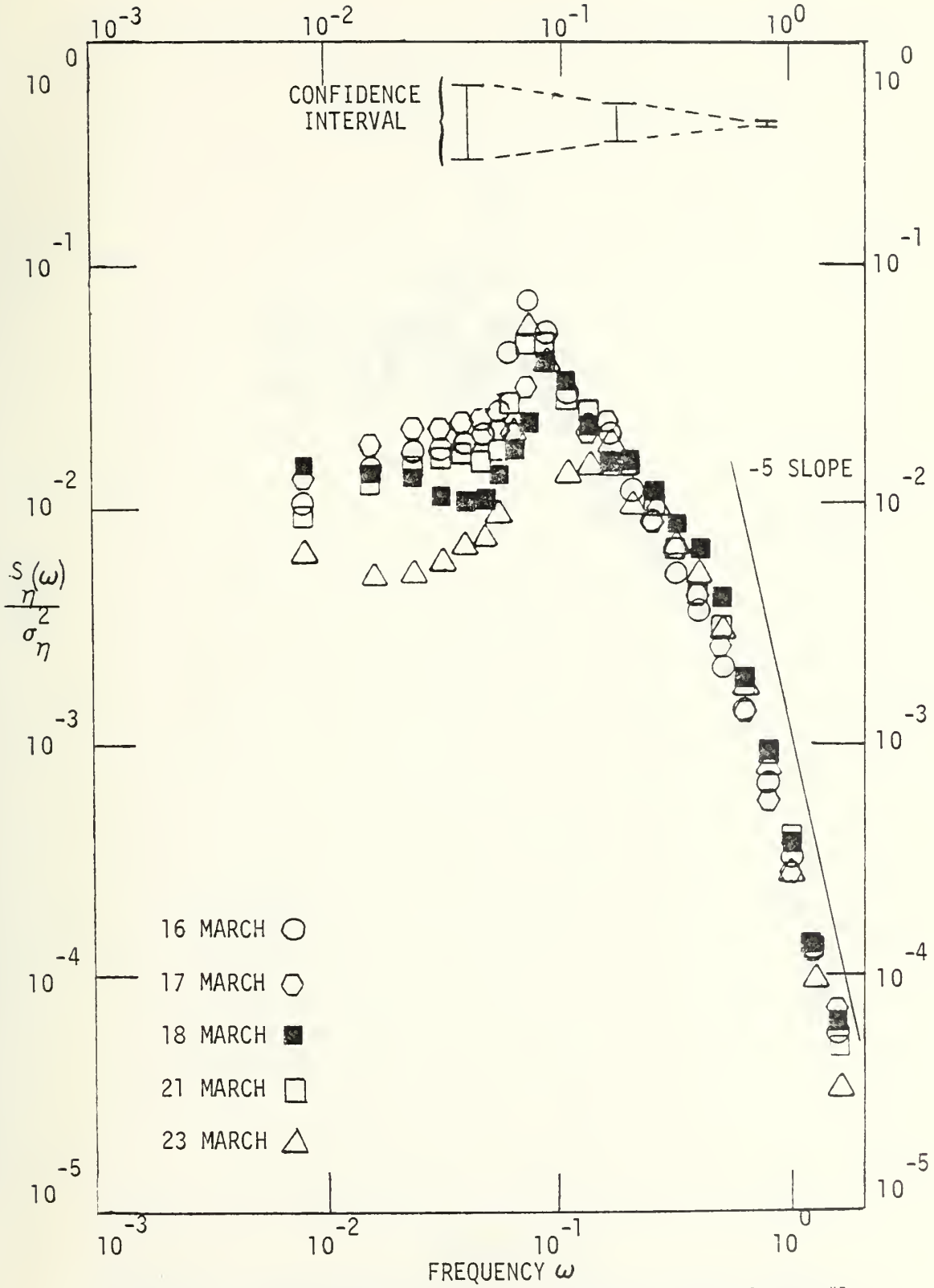

Figure 10. Sea Surface Elevation spectra at Wave Gauge #1.

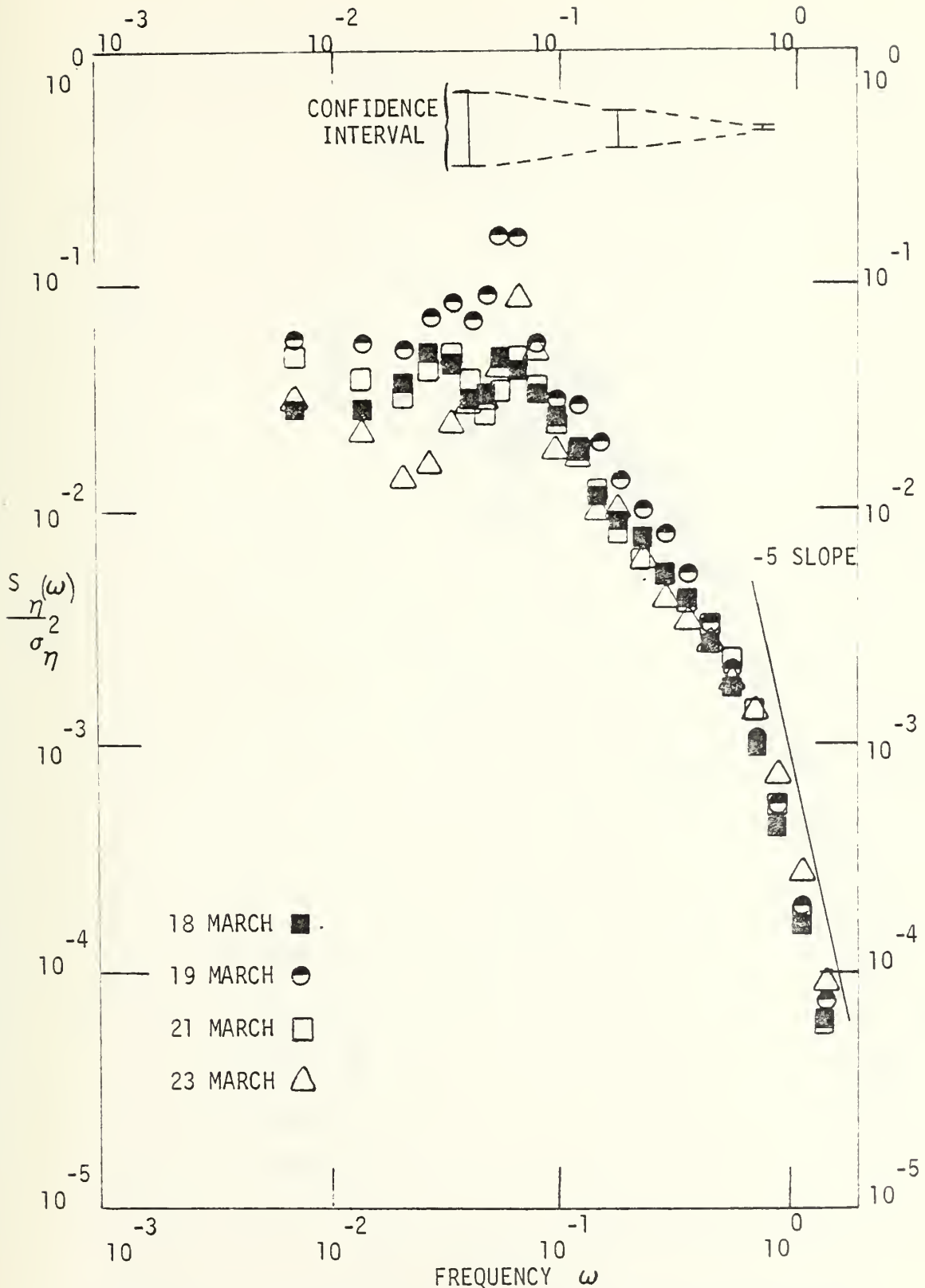

Figure 11. Sea Surface Elevation spectra at Wave Gauge #3

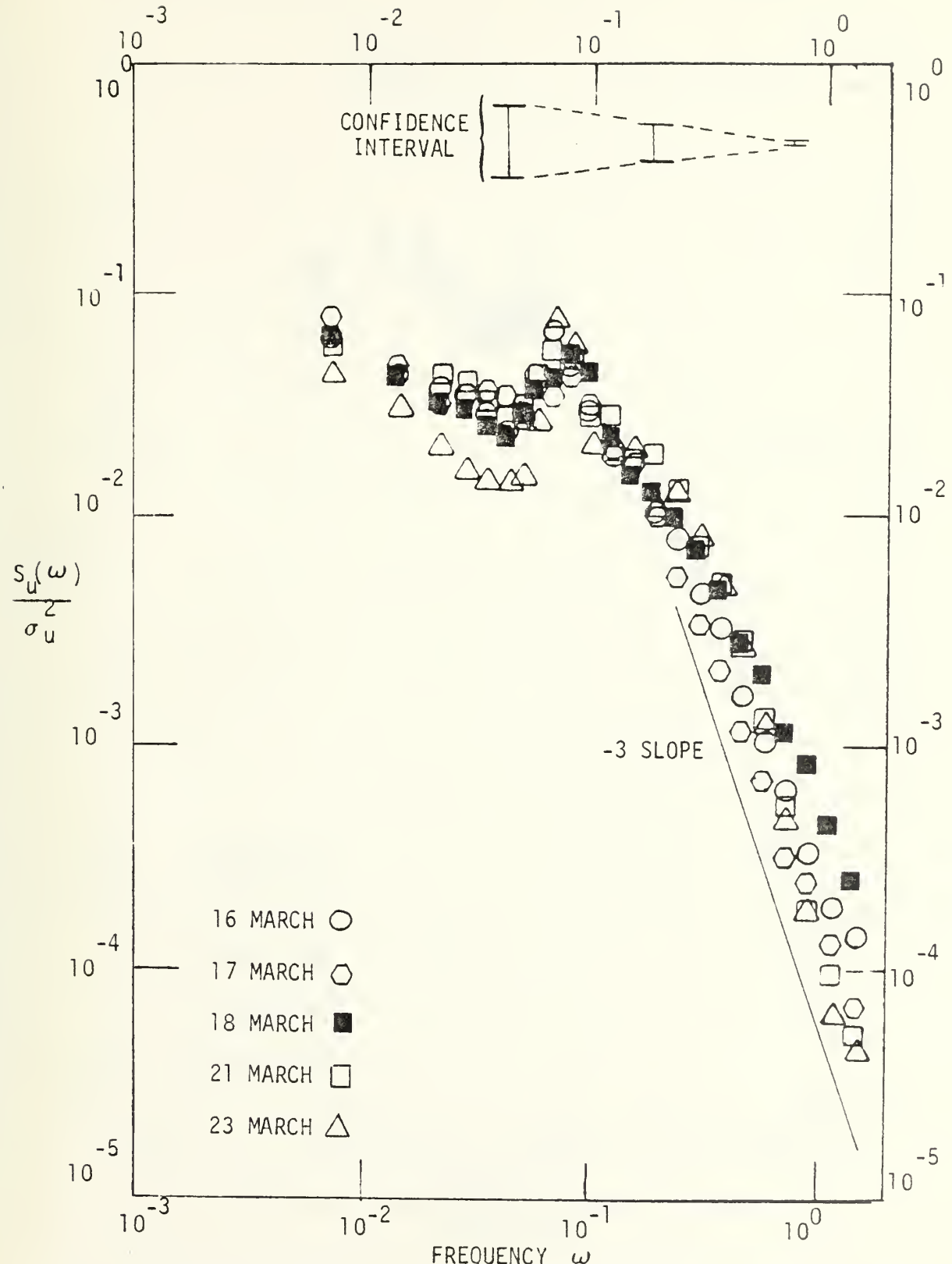

Figure 12. Onshore water particle velocity spectra at Flow Meter #1.

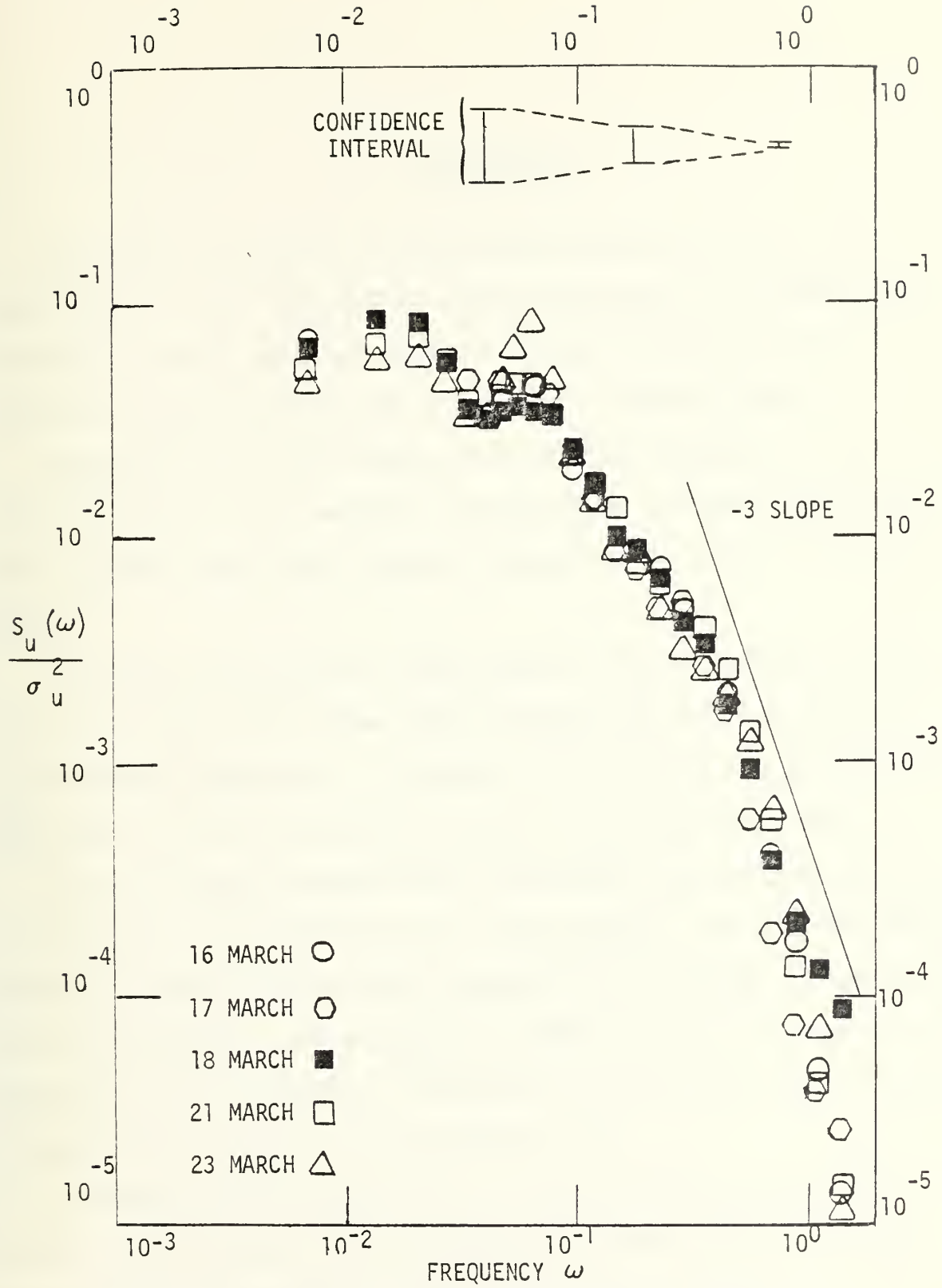

Figure 13. Onshore water particle velocity spectra at Flow Meter #3.

V. CONCLUSIONS

The values of the pdf's of sea surface elevation were positively skewed verifying the asymmetrical shape of the waves in the breaker zone. On the other hand, the skewness of the velocity components were both positive and negative and presented no readily apparent pattern.

The mean values of the onshore and alongshore components of flow indicated the presence of a nearshore circulation cell probably associated with the rip current which was frequently observed to the south of the instruments.

The values of the velocity energy-density spectral components calculated from wave spectra using linear theory indicate a qualitative, but not quantitative, relationship. In general, linear theory overestimated the magnitude of the velocity spectra because of wave directionality.

The high coherence between waves and onshore flow indicated that most of the motion in the breaking wave is wave-induced. The coherence between waves and onshore flow was used to separate the turbulence to wave-induced velocity components. The measurements showed that over the range of collapsing to spilling breakers a reasonable value for the ratio of turbulent to wave-induced velocity is approximately 0.75.

The waves lead the onshore flow in spectral phase on the average by less than 20 degrees, implying that the "curling" crest of the wave arrives prior to maximum water particle velocity.

The wave and velocity energy-density spectra at higher frequencies exhibited slopes of -5 and -3, respectively. This is indicative of deep

water wave conditions. A possible explanation for the surprising spectral slope is that most of the waves measured were either spilling breakers or reformed waves. It may be that the measured waves did not attain saturation conditions during breaking, as do plunging and collapsing breakers.

APPENDIX A

BEACH PROFILES AT TORREY PINES BEACH 16-23 MARCH 1977

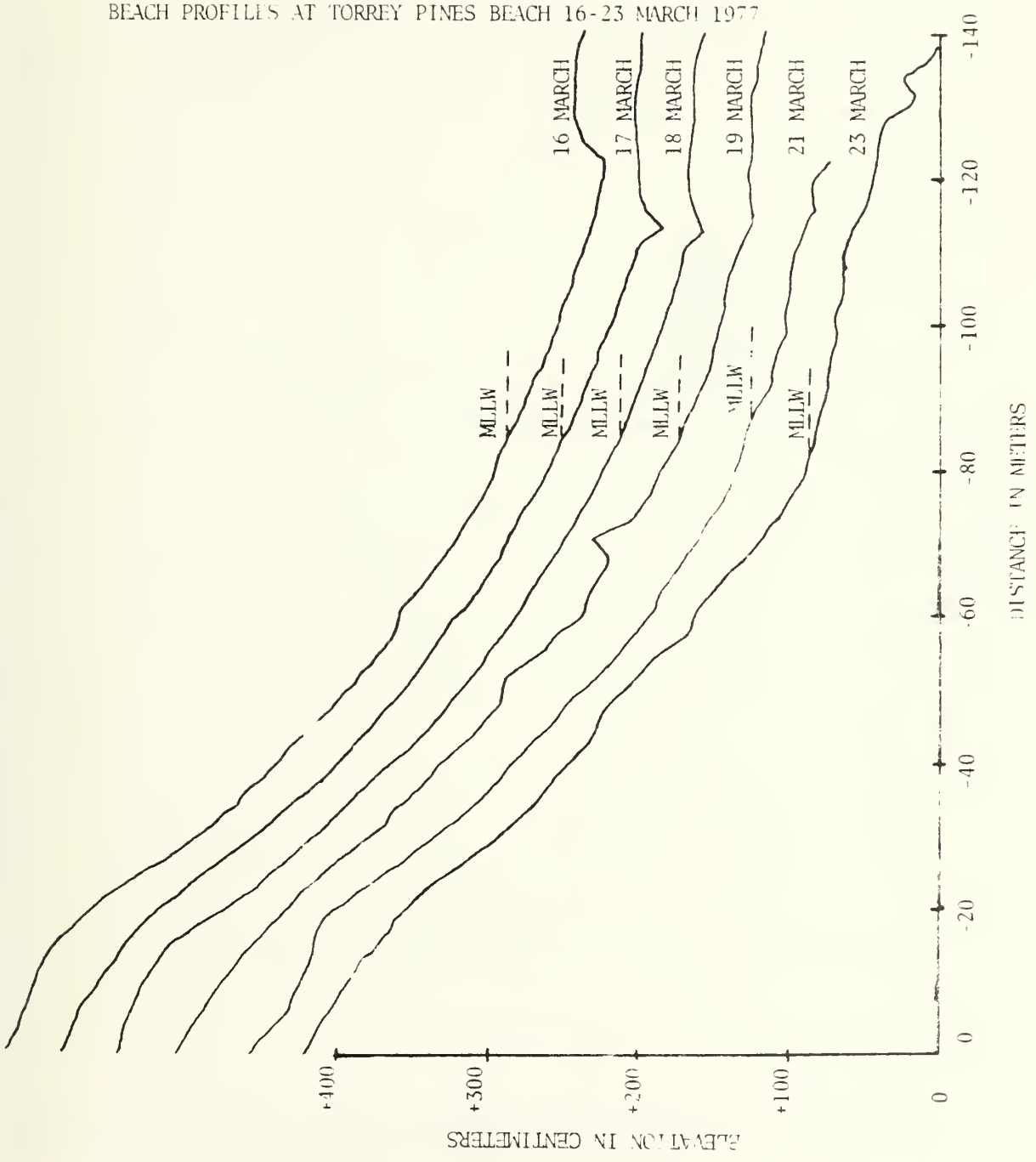

APPENDIX B

CAPACITANCE WAVE GAUGE CALIBRATIONS

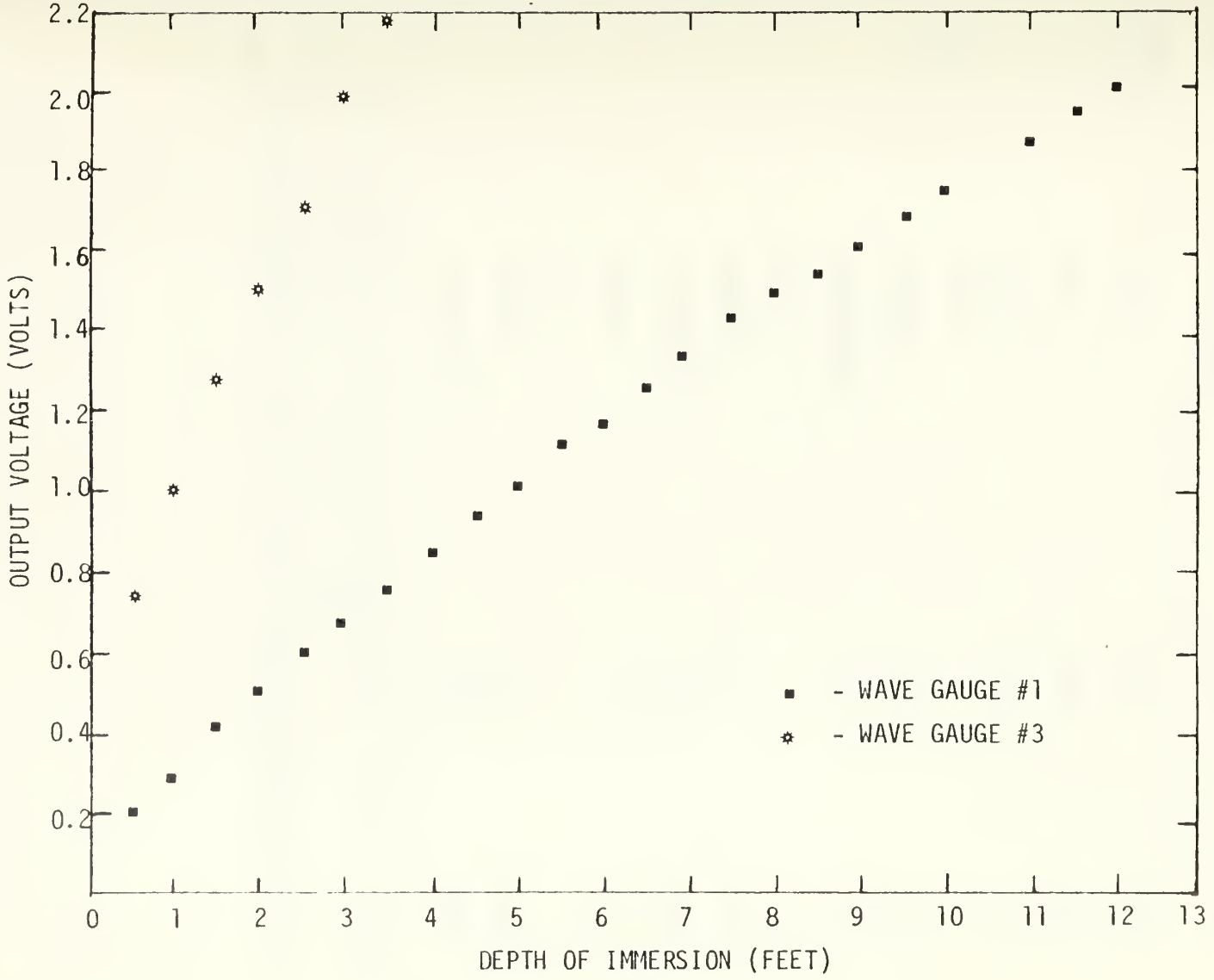

APPENDIX C

CALIBRATION FACTORS

DATE	INSTRUMENT	CALA*	CALM**
MARCH 16,21,23	WG #1	-1.154	.00474
17,19	WG #1	-1.284	.00503
18	WG #1	-1.453	.00520
ALL DATES	FM #1		
	ONSHORE	.009	.00764
	ALONGSHORE	- .006	.00747
	FM #2		
	ONSHORE	+ .131	-.00911
	ALONGSHORE	- .084	-.00818
	WG #3	- .2798	.00156
	FM #3		
	ONSHORE	.007	-.00820
	ALONGSHORE	.006	.00763

*Calibration Additive Factor for wave heights is given in meters; CALA for flow is given in meters per second.

**Calibration Multiplication Factor for wave heights is given in meters per bit; CALM for flows is given in meters per second per bit.

APPENDIX D

PROBABILITY DENSITY FUNCTIONS VS. GRAM-CHARLIER DISTRIBUTIONS

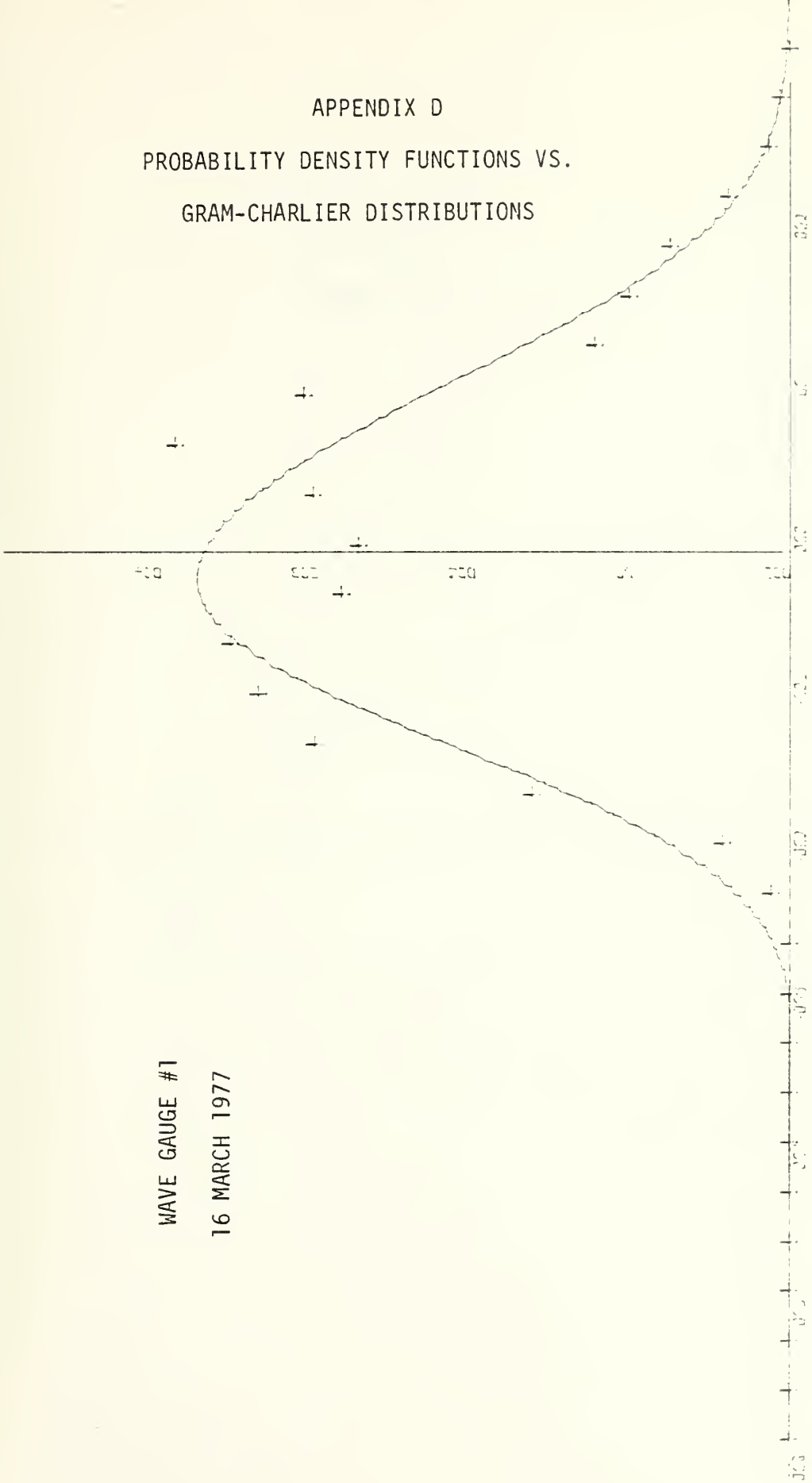

WAVE GAUGE #1

16 MARCH 1977

Onshore Flow at

FLOW METER #1

16 MARCH 1977

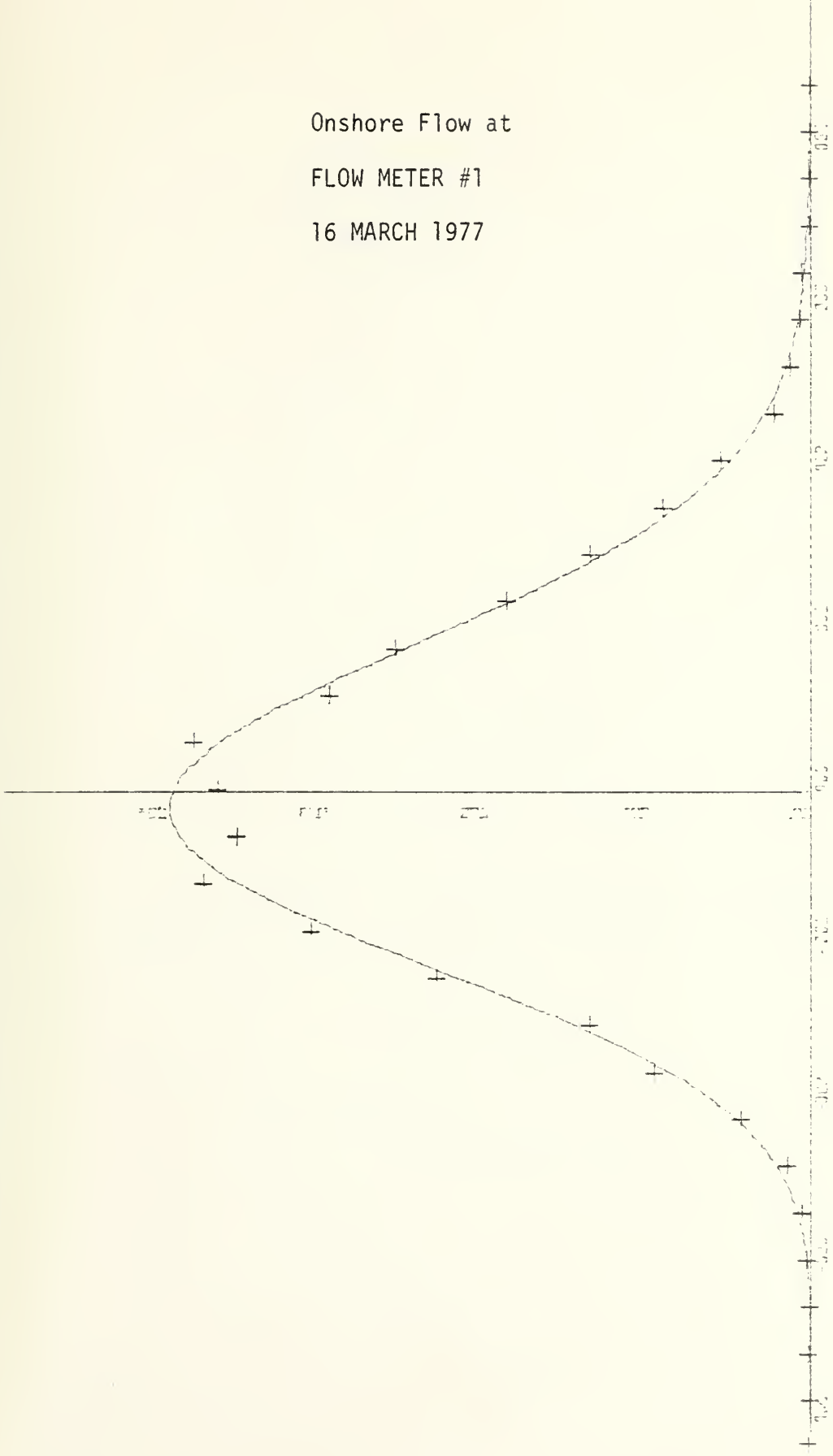

WAVE GAUGE #1

17 MARCH 1977

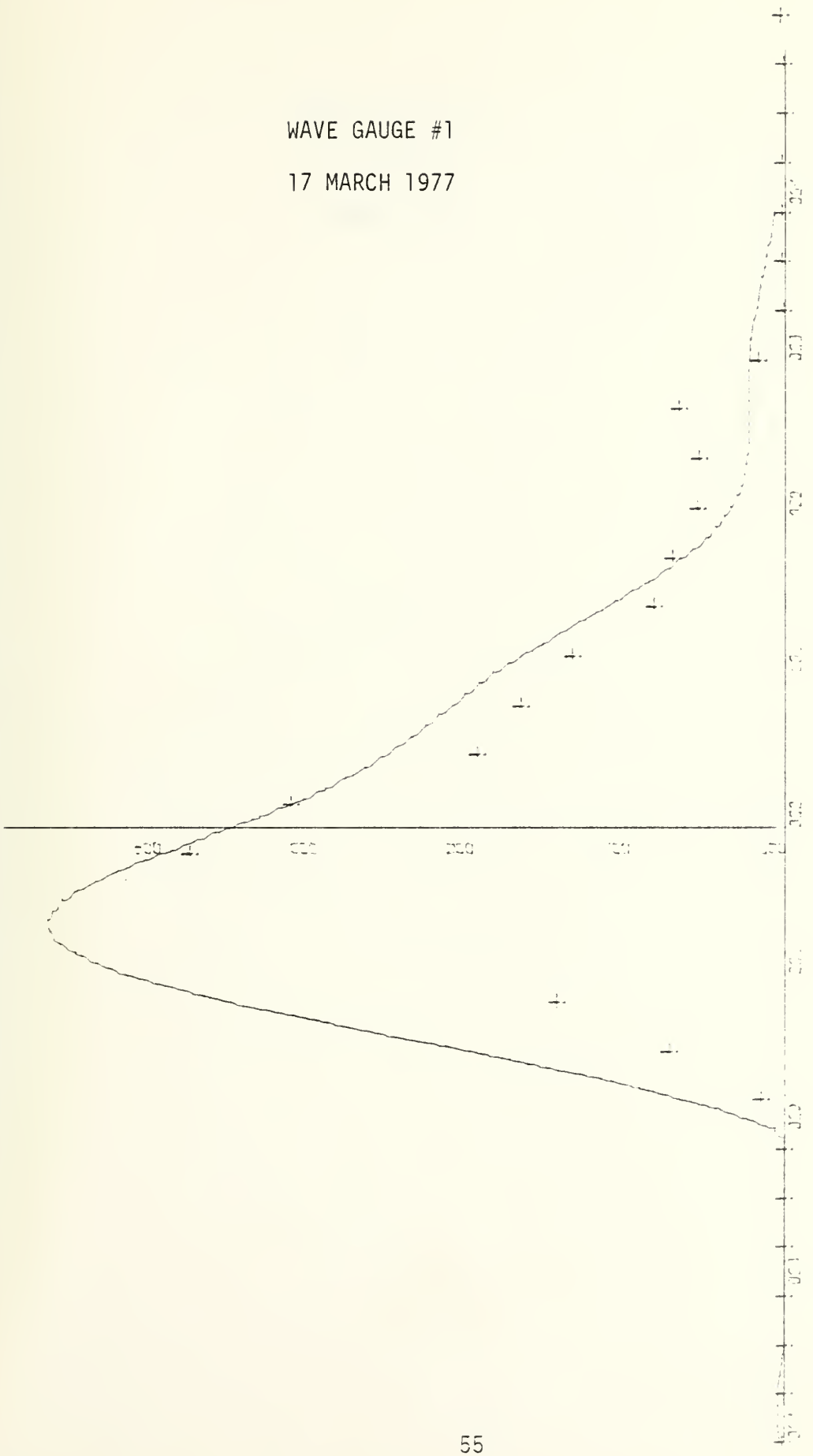

Onshore Flow at

FLOW METER #1

17 MARCH 1977

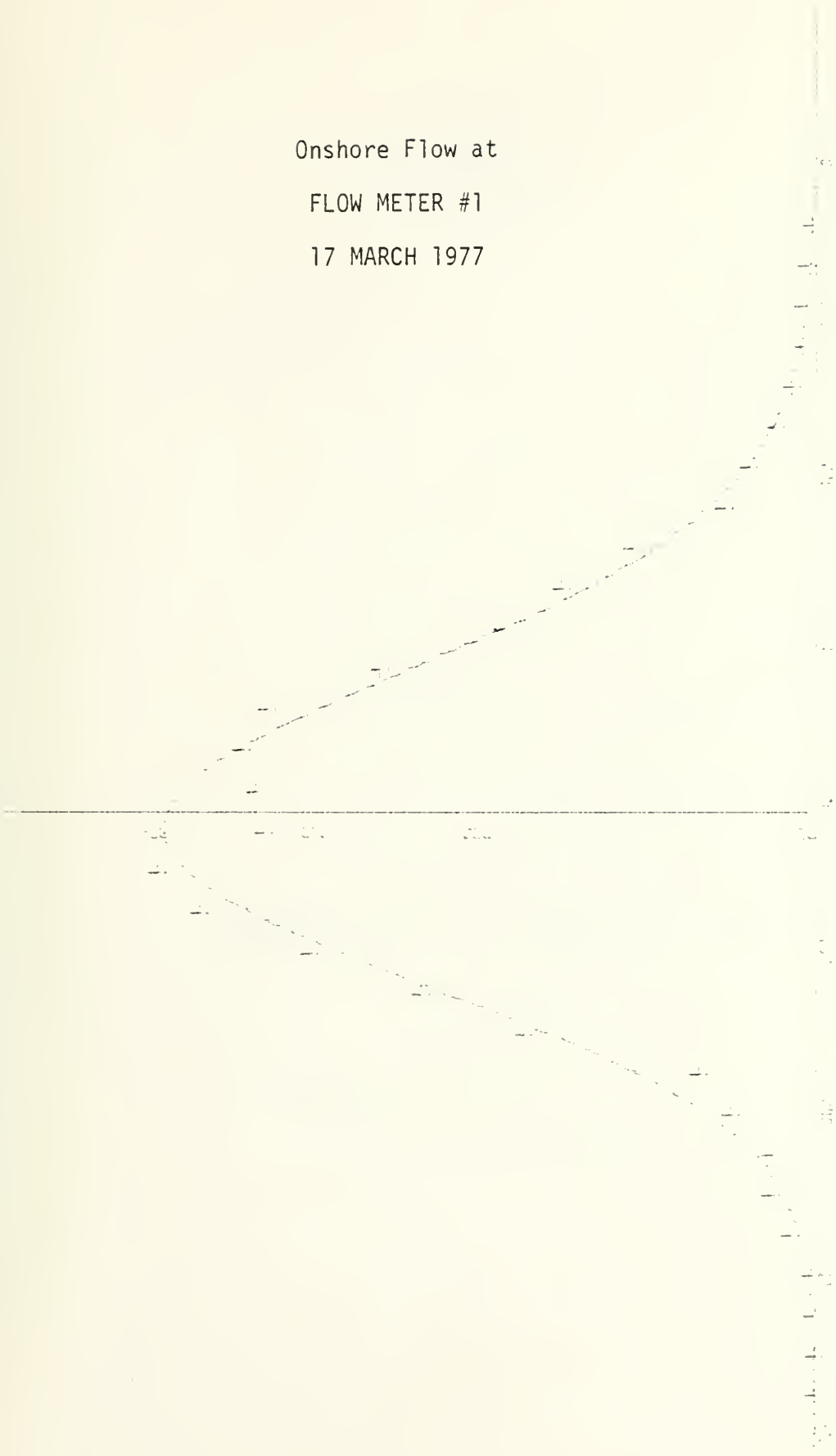

WAVE GAUGE #1

18 MARCH 1977

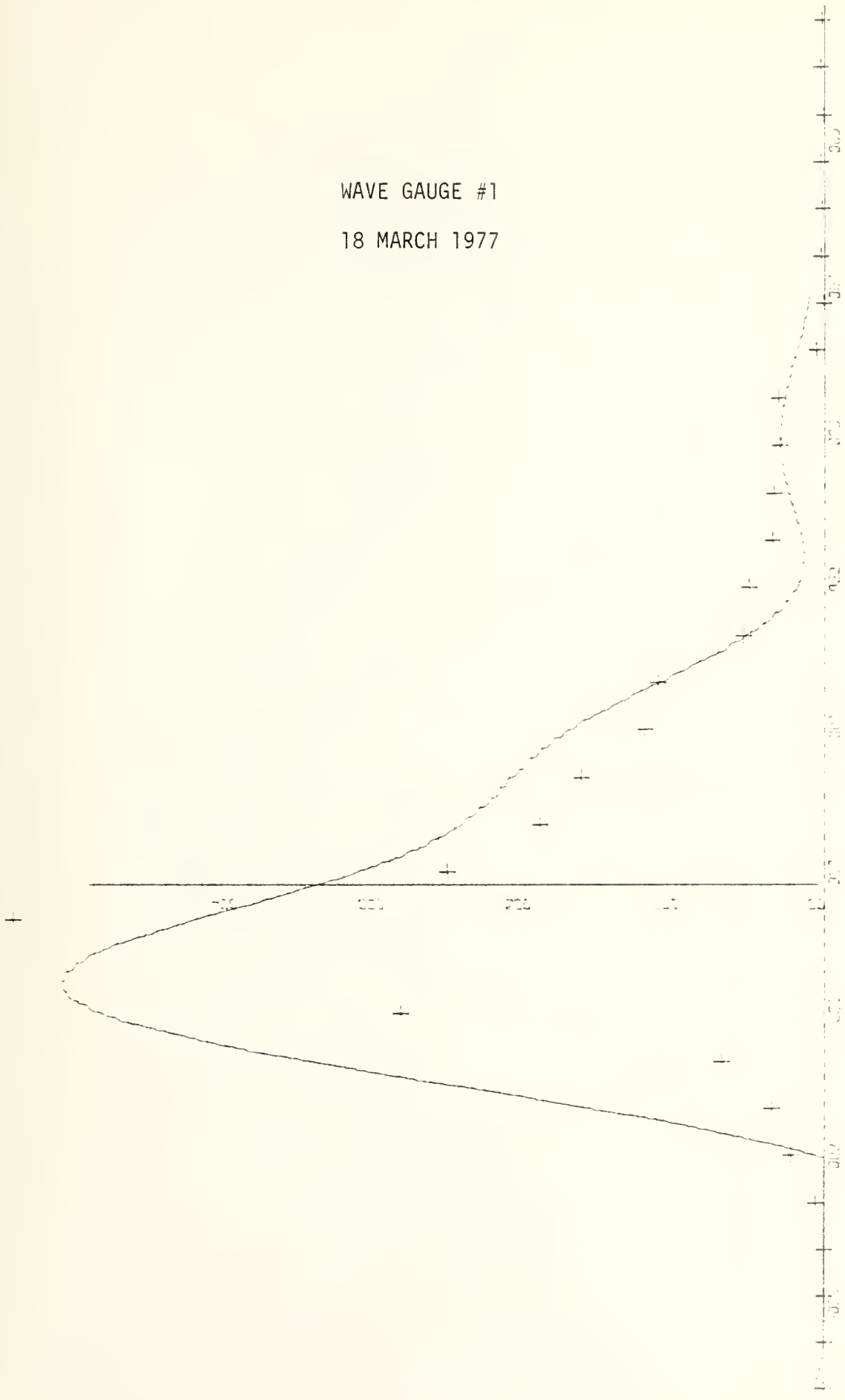

Onshore Flow at

FLOW METER #1

18 MARCH 1977

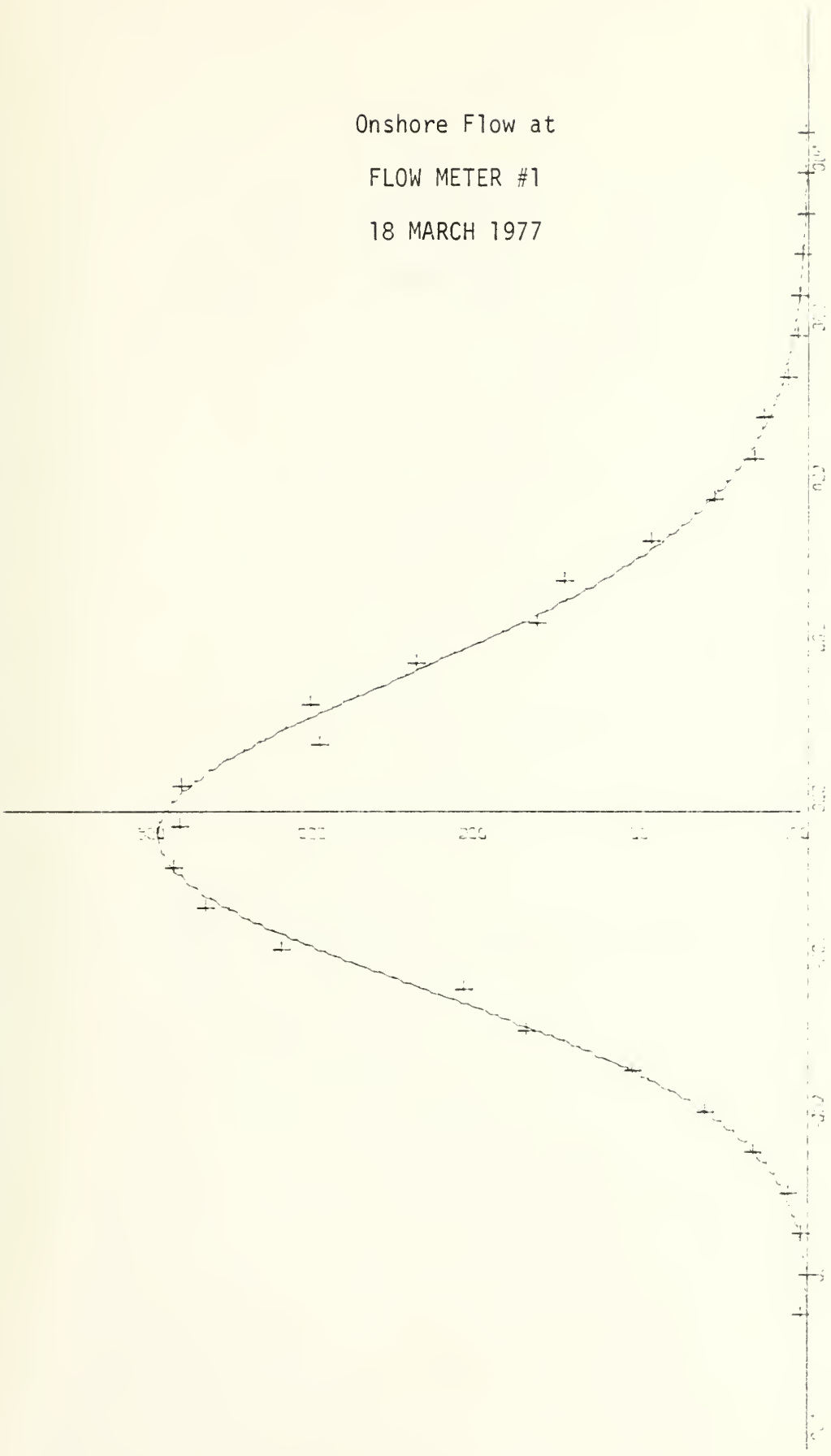

WAVE GAUGE #1

21 MARCH 1977

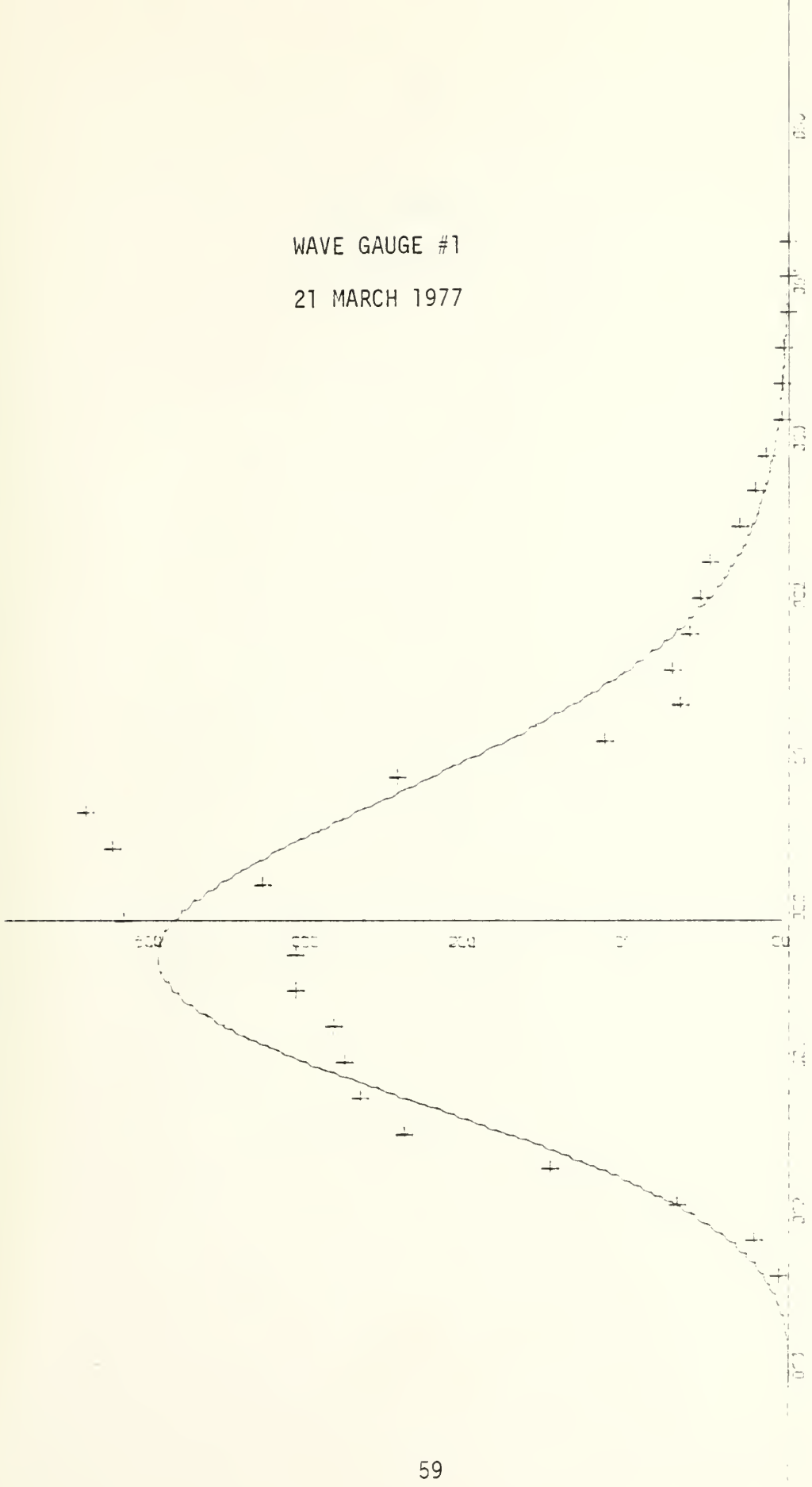

WAVE GAUGE #1

23 MARCH 1977

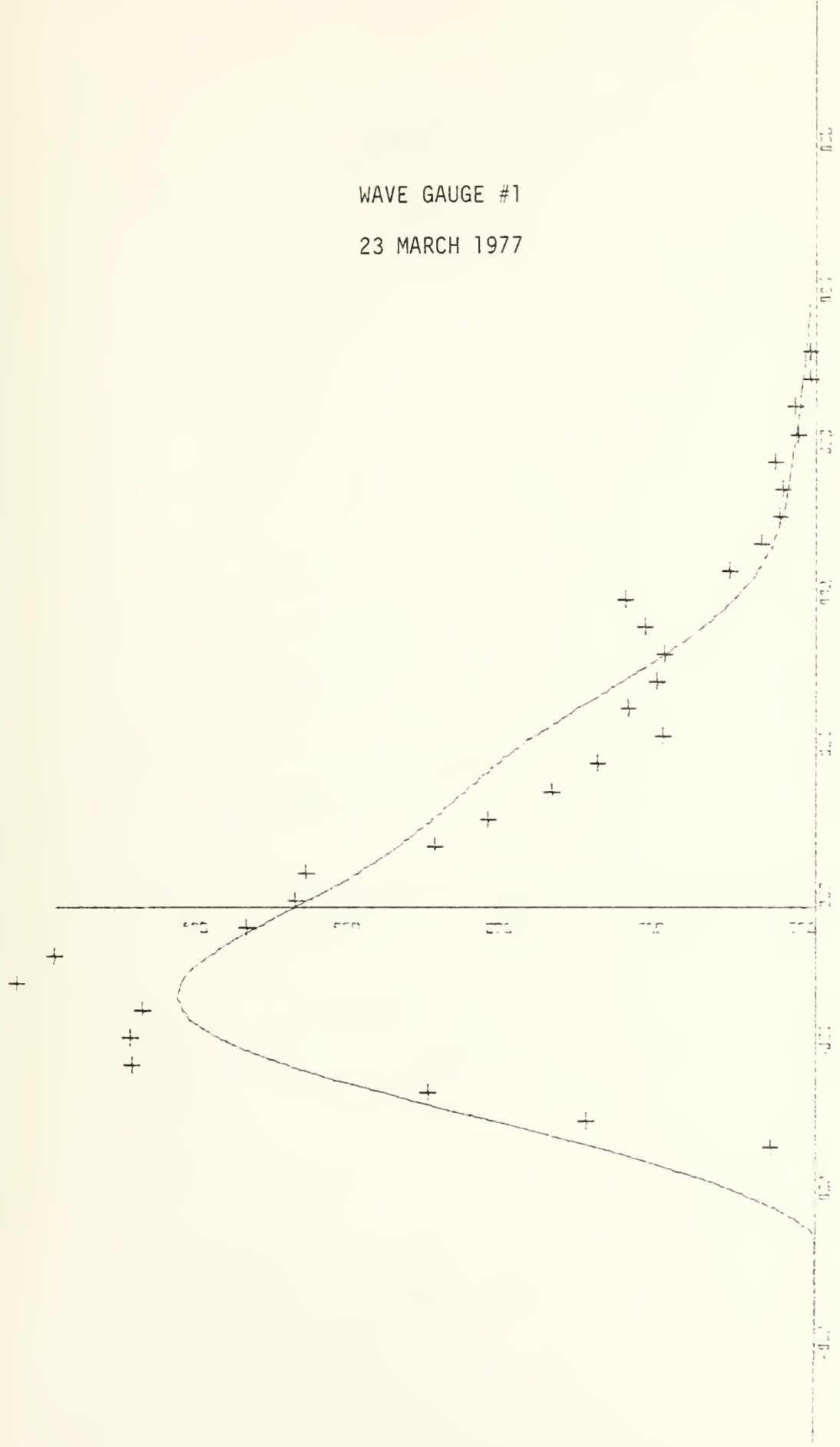

WAVE GAUGE #3

18 MARCH 1977

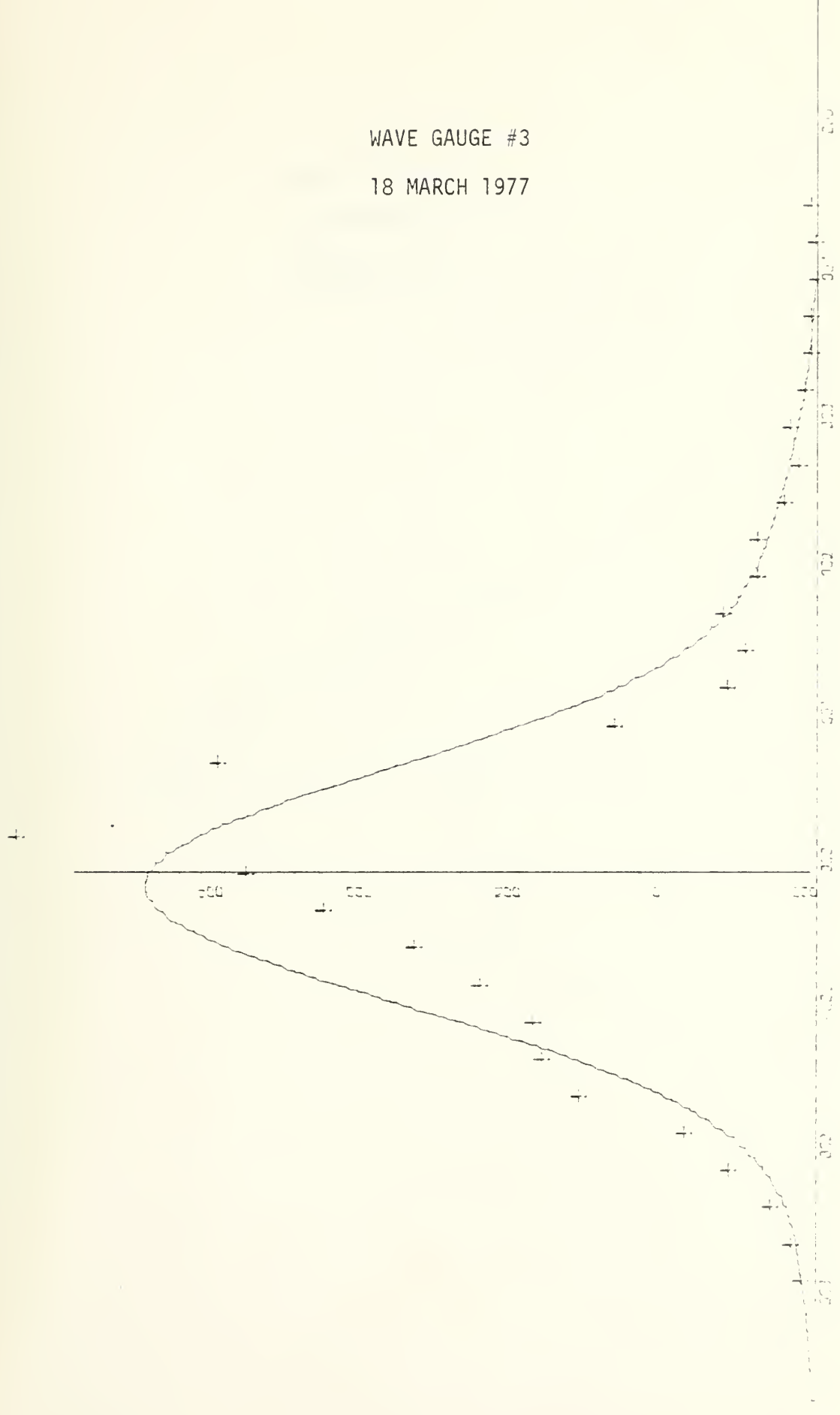

Onshore Flow at

FLOW METER #3

18 MARCH 1977

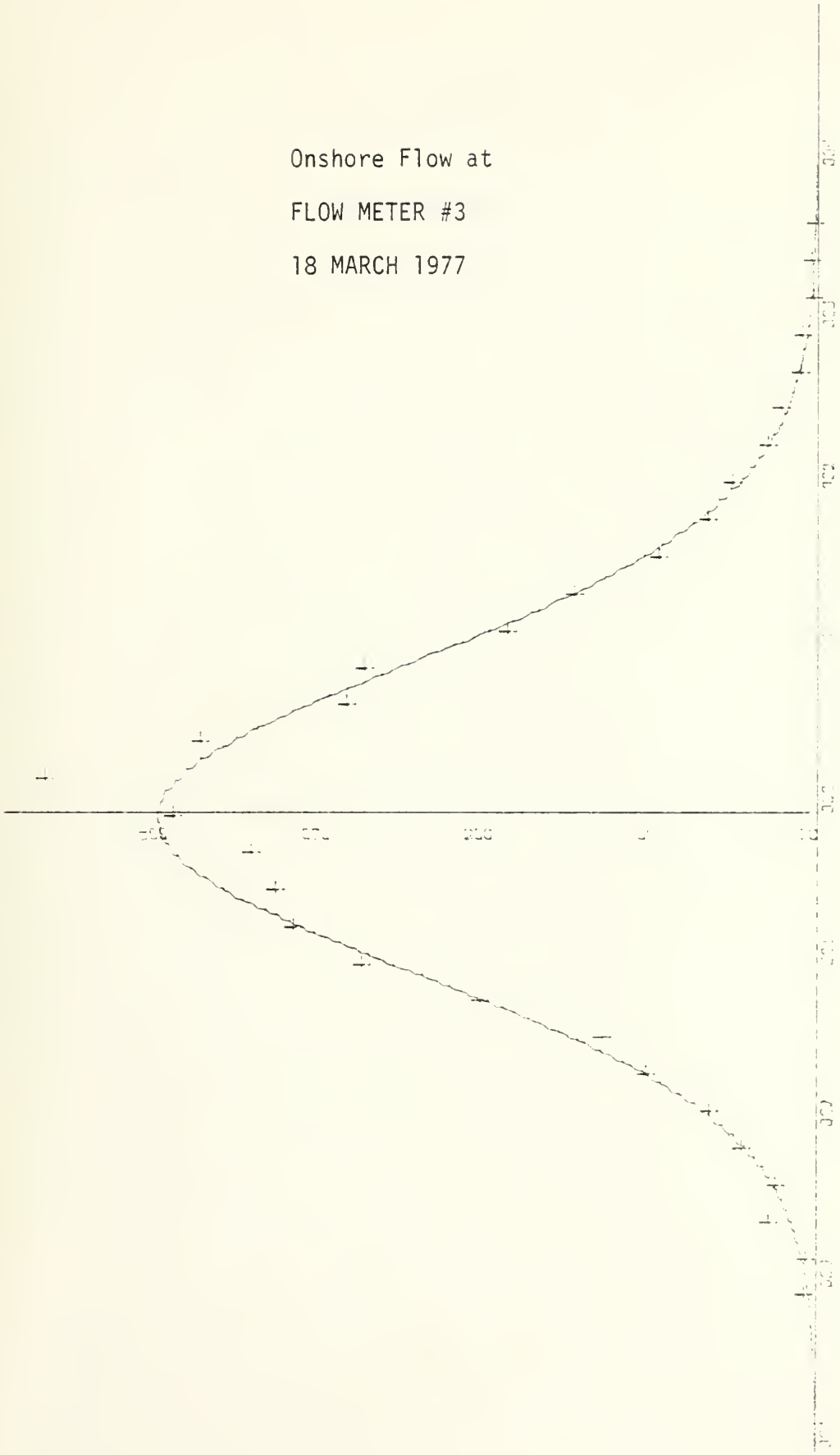

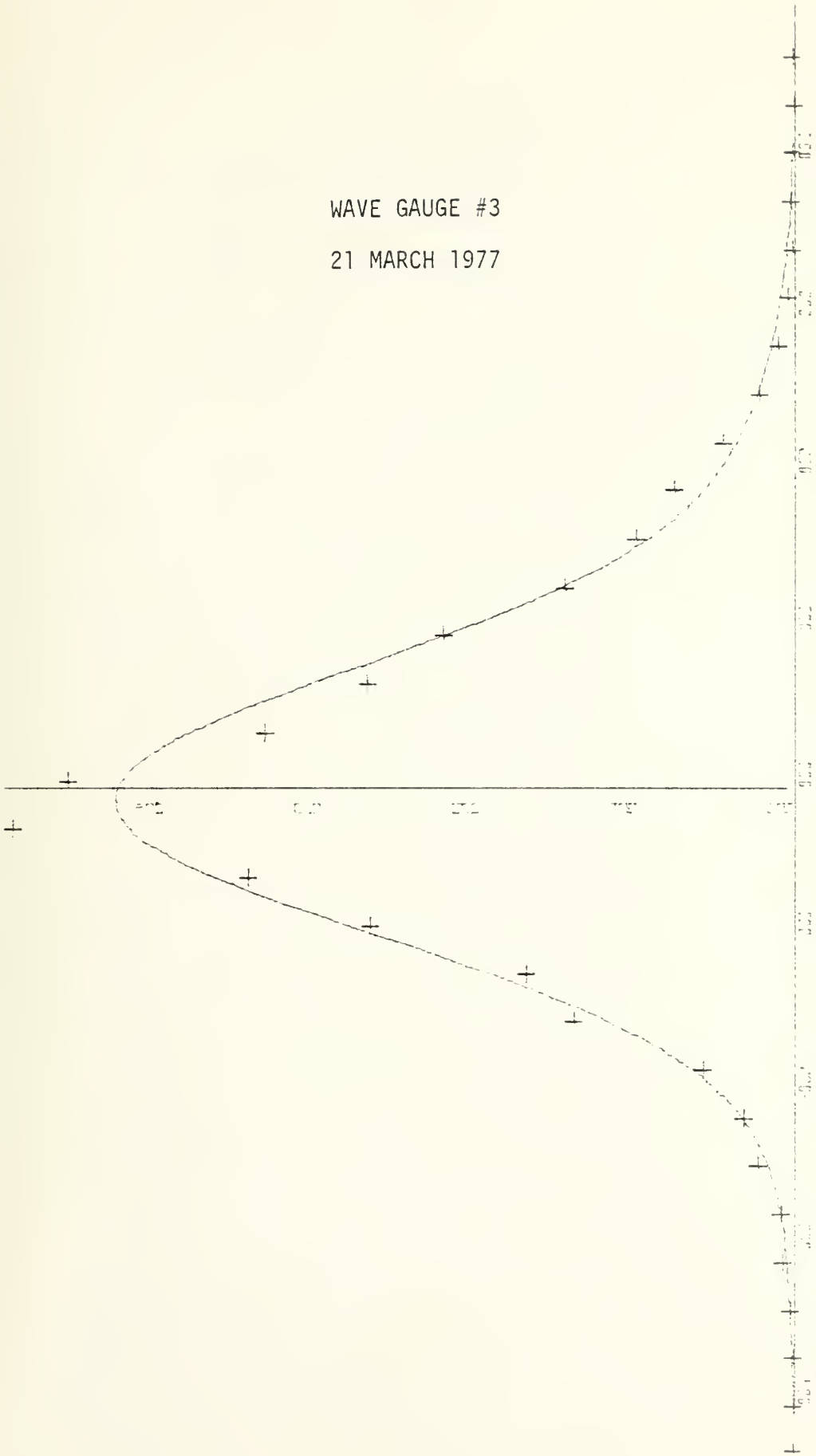
WAVE GAUGE #3
21 MARCH 1977

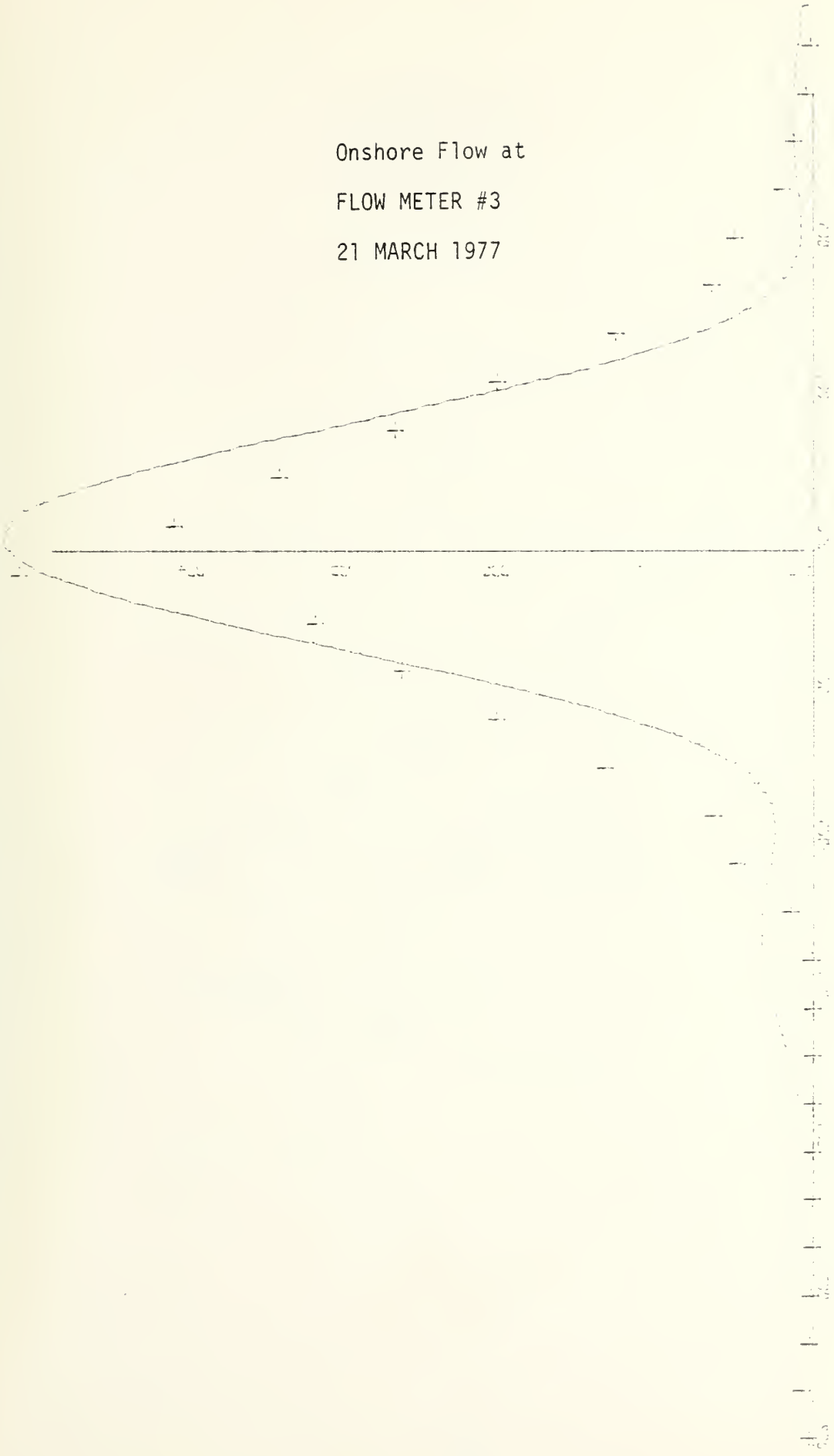
Onshore Flow at
FLOW METER #3
21 MARCH 1977

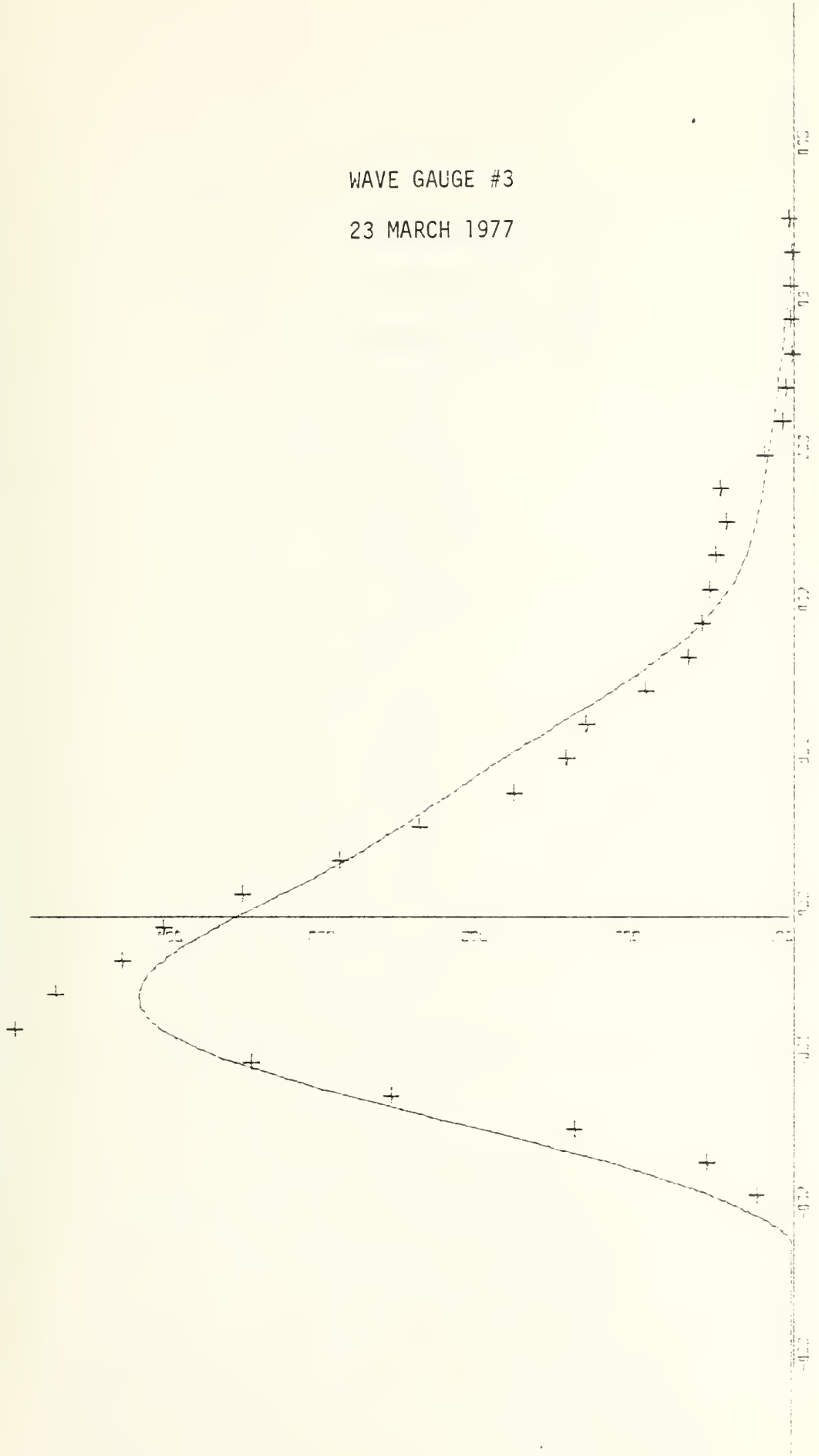
WAVE GAUGE #3
23 MARCH 1977

Onshore Flow at

FLOW METER #3

23 MARCH 1977

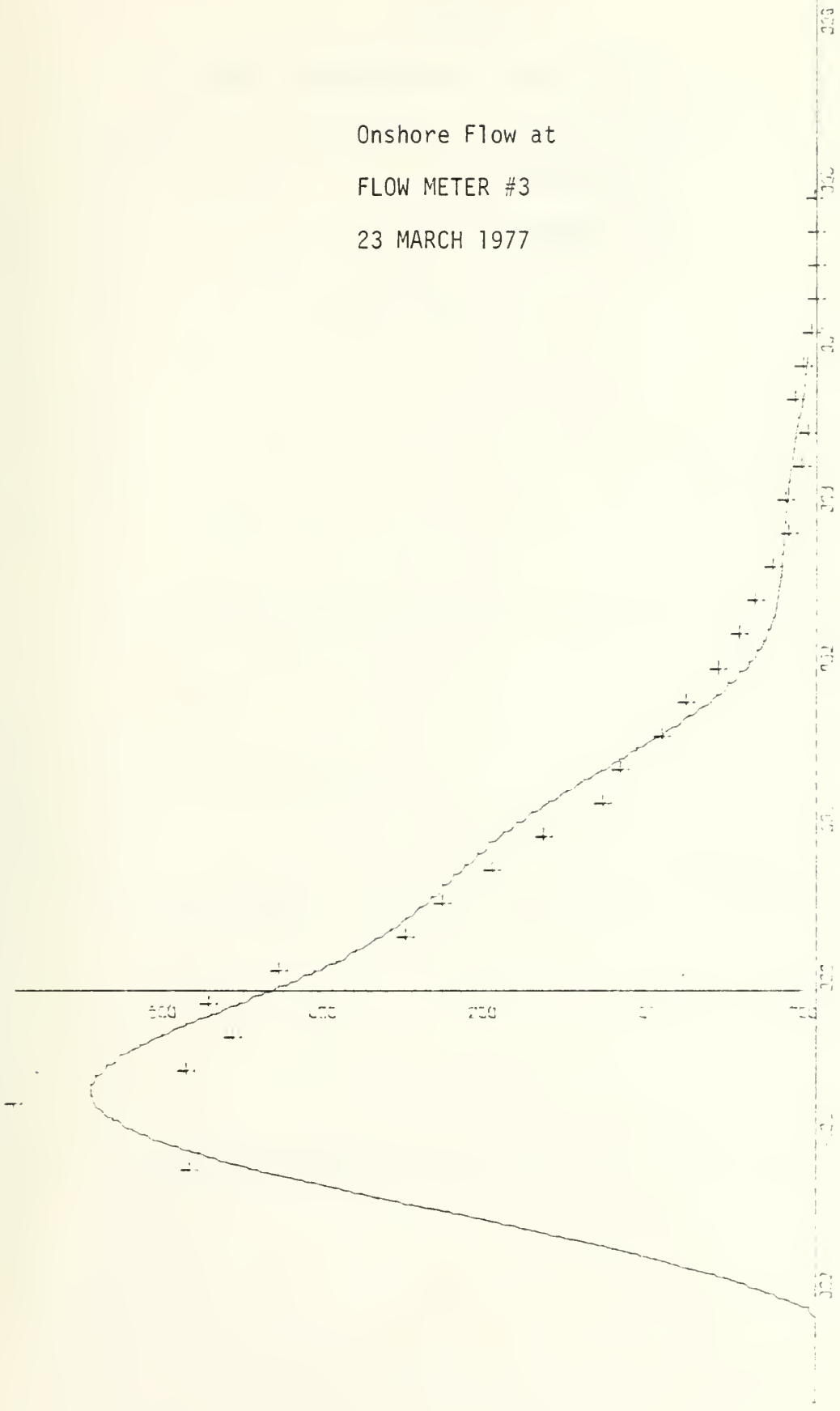

APPENDIX E

POWER COHERENCE AND PHASE SPECTRA

WAVE GAUGE #1 - Onshore Flow at

FLOW METER #1

16 MARCH 1977

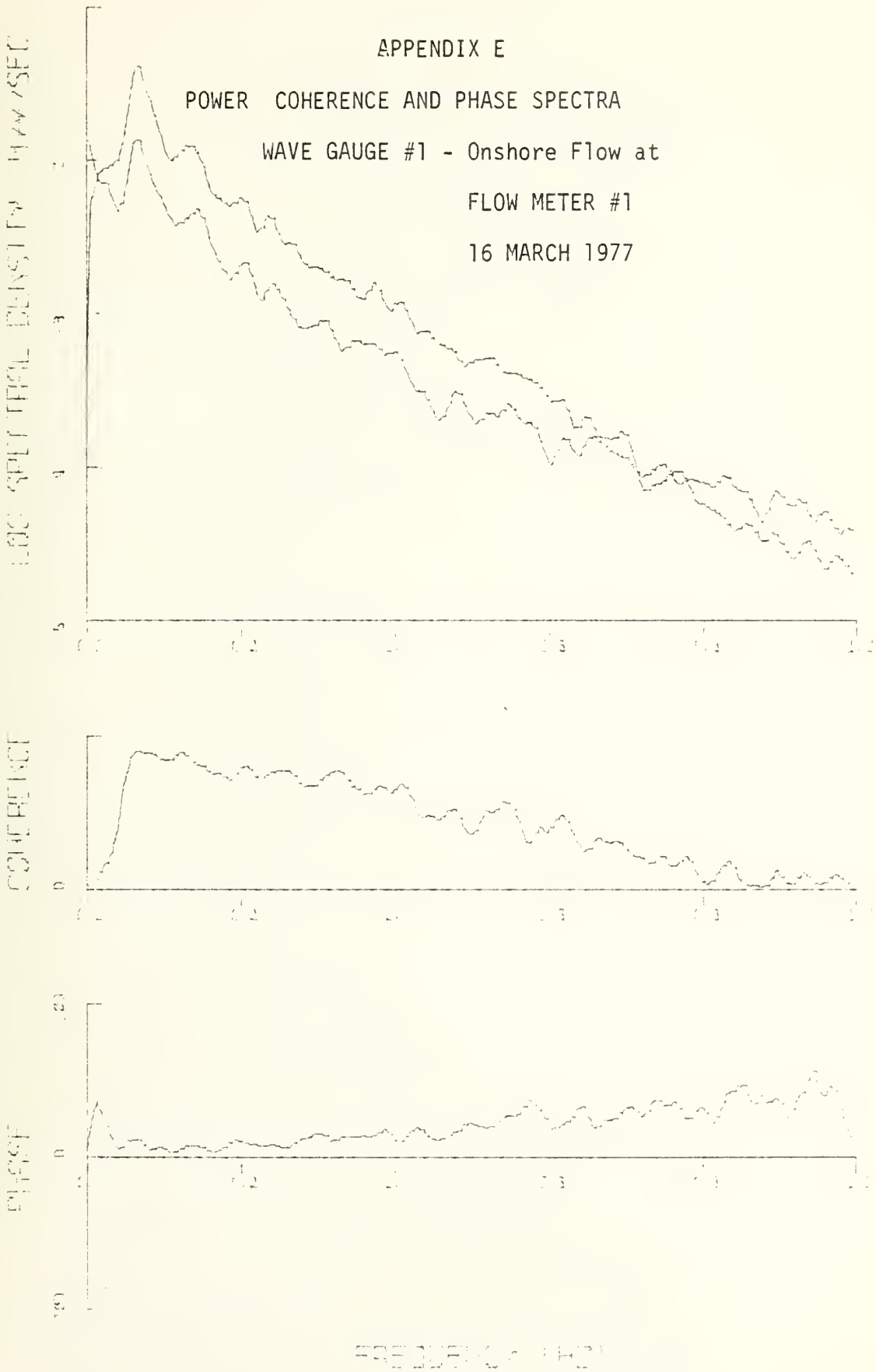

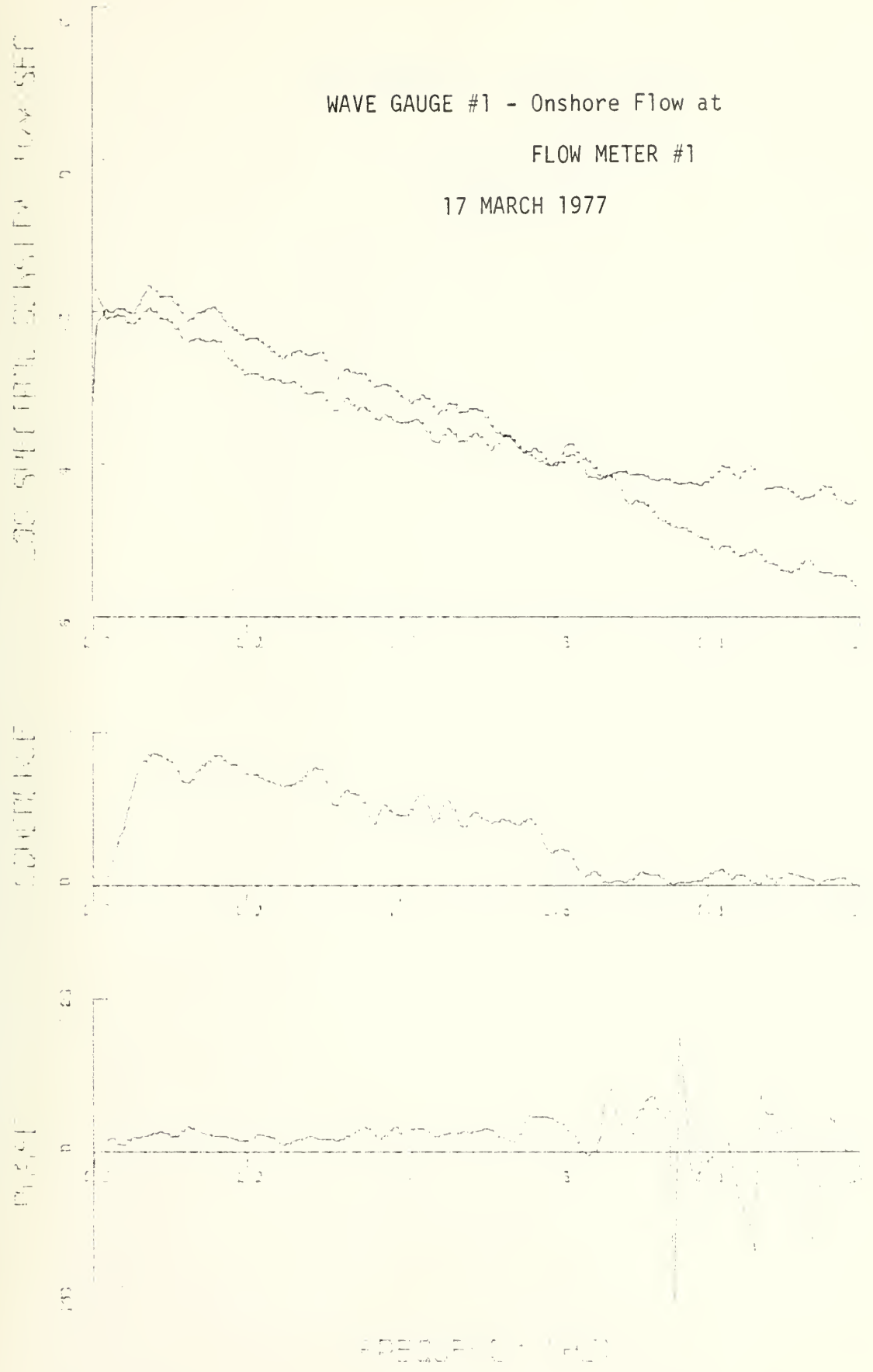
WAVE GAUGE #1 - Onshore Flow at
FLOW METER #1
17 MARCH 1977

WAVE GAUGE #1 - Onshore Flow at

FLOW METER #1

18 MARCH 1977

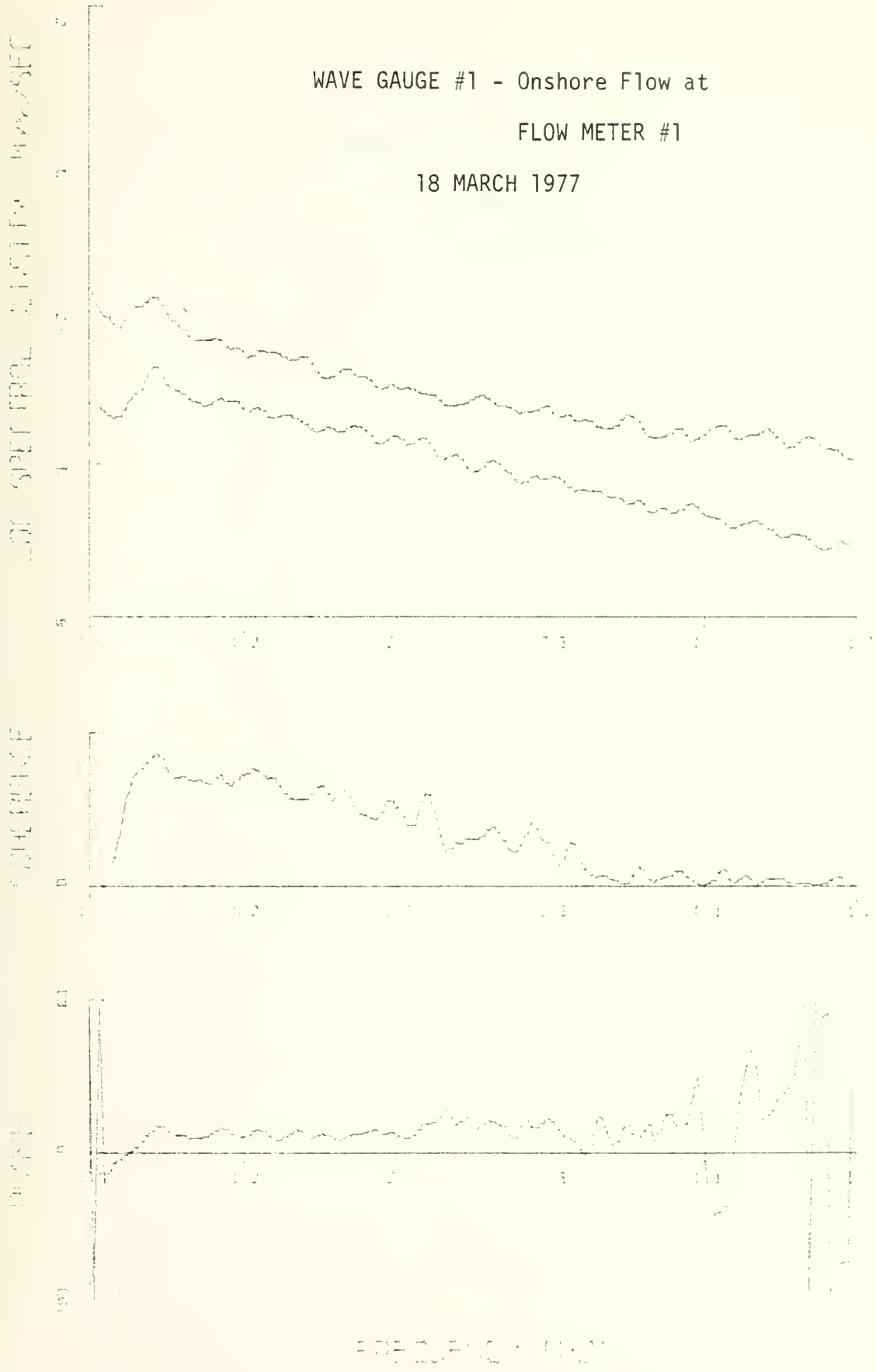


WAVE GAUGE #1 - Onshore Flow at
FLOW METER #1
21 MARCH 1977

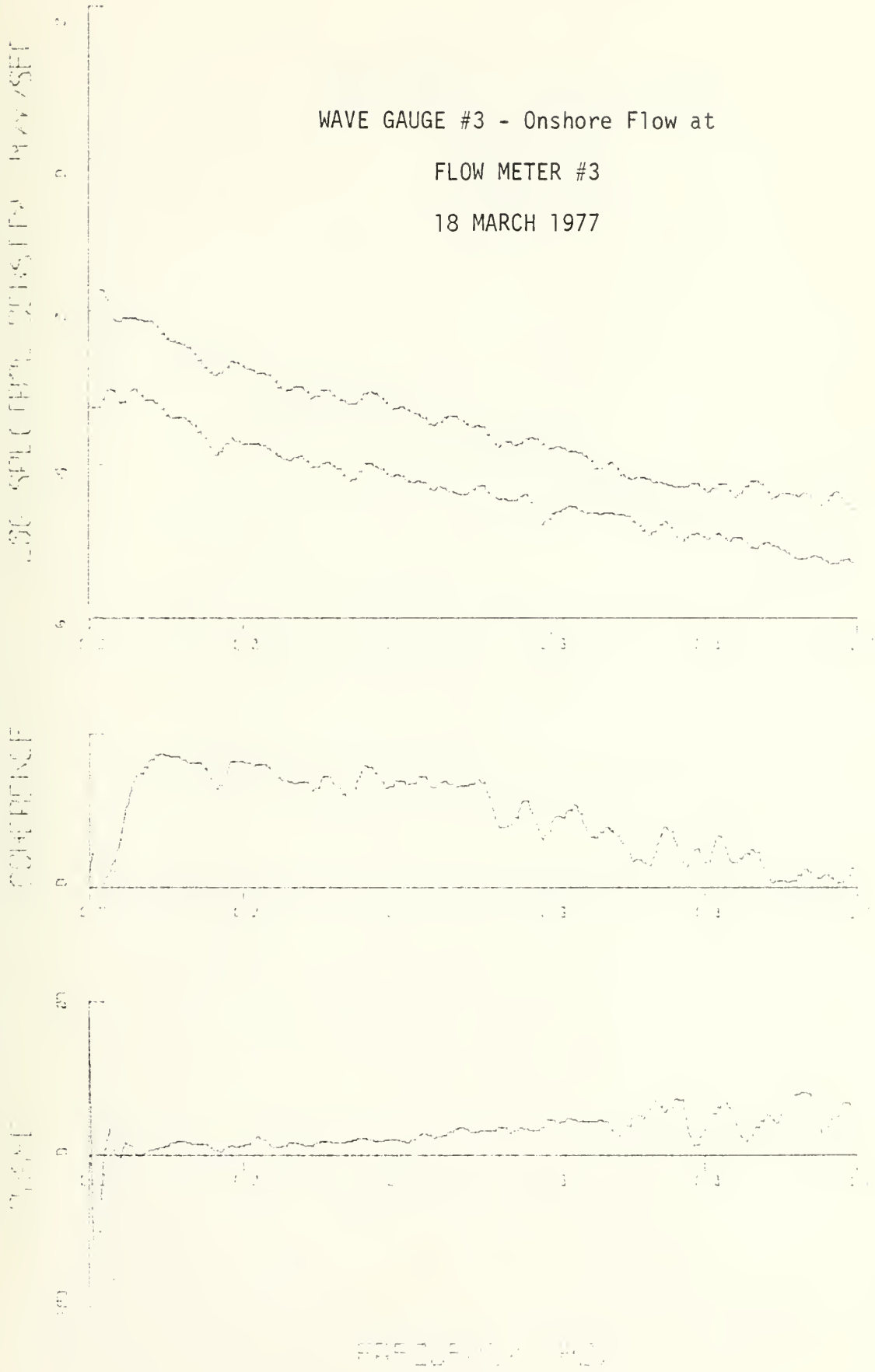
WAVE GAUGE #3 - Onshore Flow at
FLOW METER #3
18 MARCH 1977

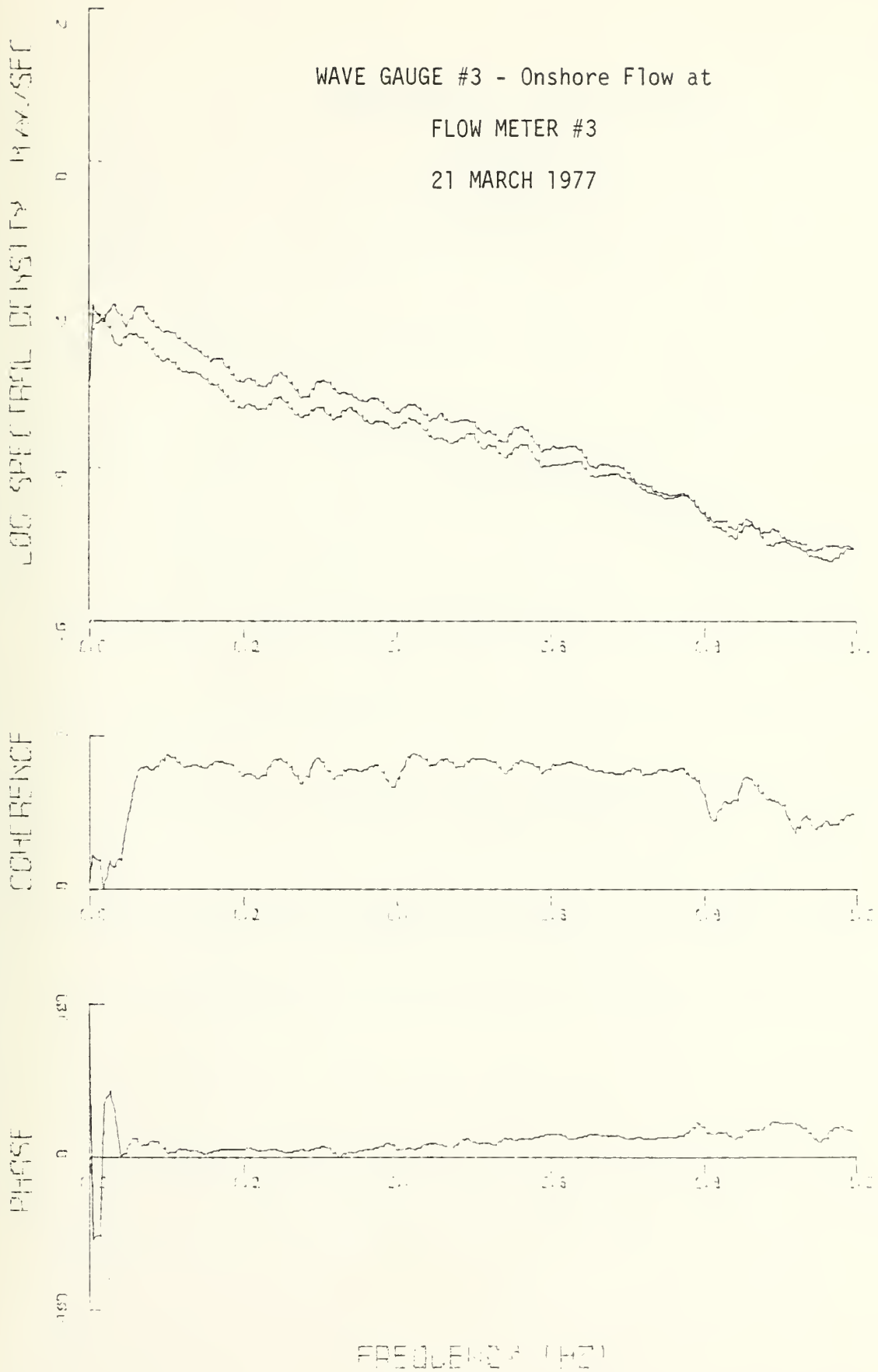
WAVE GAUGE #3 - Onshore Flow at
FLOW METER #3
21 MARCH 1977
COHERENCE
PHASE

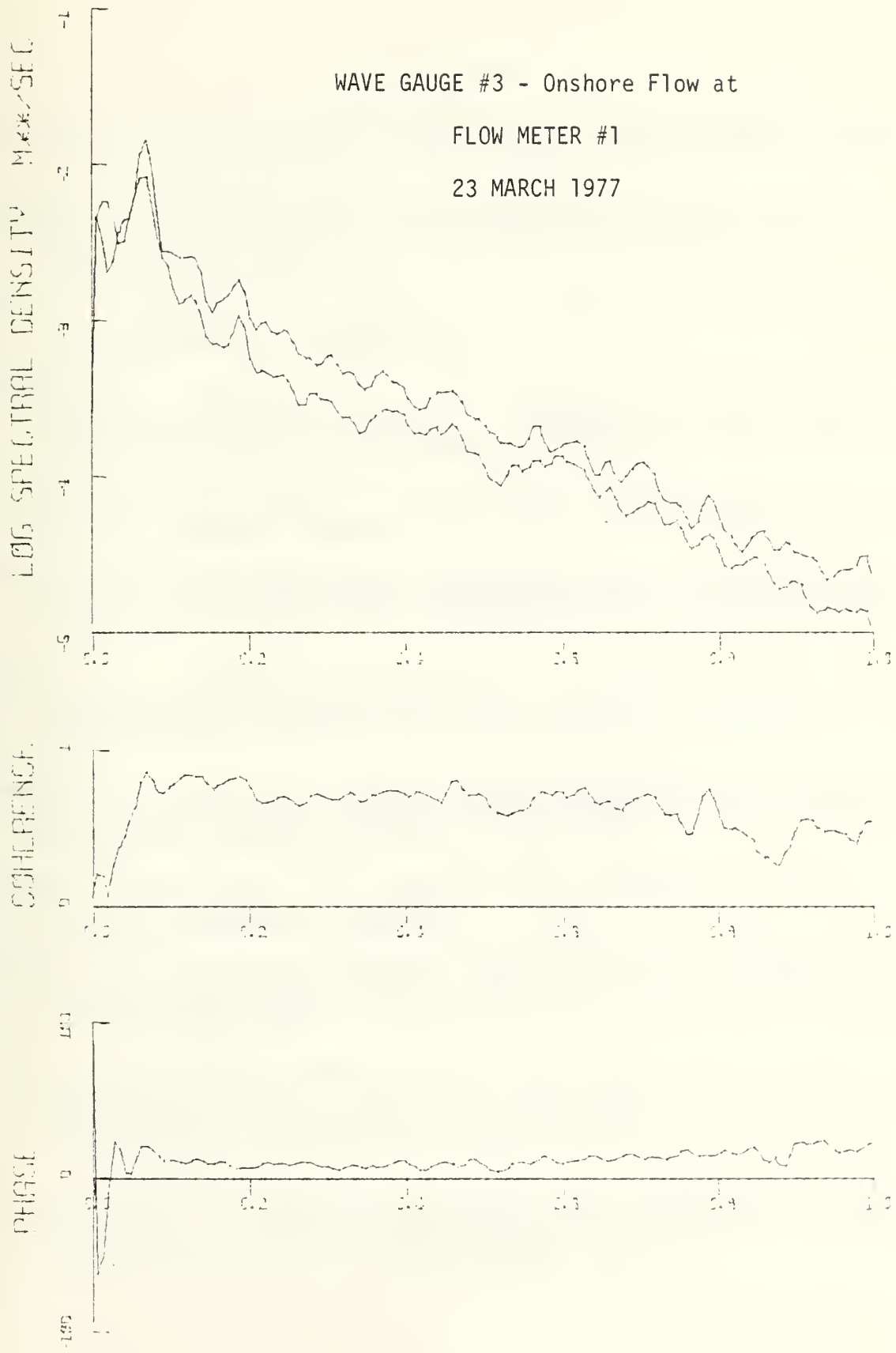
WAVE GAUGE #3 - Onshore Flow at
FLOW METER #1
23 MARCH 1977
LOG SPECTRAL DENSITY M**2/SEC
COHERENCE
PHASE

BIBLIOGRAPHY

Battjes, J., "Surf Similarity," Proceedings of the Fourteenth Conference on Coastal Engineering, pp. 466-479, ASCE, 1974.

Bowen, A.J. and Huntley, D.A., "Field Measurements of Nearshore Velocities," Proceedings of the Fourteenth Conference on Coastal Engineering, pp. 538-557, ASCE, 1974.

Bub, F.L., Surf Zone Wave Kinematics, M.S. Thesis, Naval Postgraduate School, Monterey, California, 1974.

Führböter, A., and Büsching, F., "Wave Measuring Instrumentation for Field Investigations on Breakers," Proceedings of the International Symposium on Ocean Wave Measurements and Analysis, ASCE, 1974.

Galvin, C.J., "Wave Breaking in Shallow Water," Waves on Beaches and Resulting Sediment Transport, pp. 413-456, Academic Press, Inc., 1972.

Galvin, J.J., Kinematics of Surf Zone Breaking Waves: Measurement and Analysis, M.S. Thesis, Naval Postgraduate School, Monterey, California, 1975.

Huntley, D.H., "Lateral and Bottom Forces on Longshore Currents," Proceedings of the Fifteenth Conference on Coastal Engineering, pp. 645-659, ASCE, 1976.

Inman, D.L., and Nasu, N., Orbital Velocity Associated with Wave Action near the Breaker Zone, Technical Memorandum No. 79, U.S. Army Corps of Engineers, Beach Erosion Board, March 1956.

Inman, D.L. and Kamar, P.D., "Longshore Sand Transport on Beaches," Journal of Geophysical Research, V. 75, No. 30, October, 1971

Iverson, H.W., "Waves and Breakers in Shoaling Water," Proceedings of the Third Conference on Coastal Engineering, Council on Wave Research, pp. 1-12, ASCE, 1952.

Khristoforov, G.N. and Yefimov, V.V., "Spectra and Statistical Relations between the Velocity Fluctuations in the Upper Layer of the Sea and Surface Waves," Atmospheric and Oceanic Physics, V. 7, No. 12, pp. 1290-1310, 1971.

McGoldrick, L.F., A System for the Generation and Measurement of Capillary-Gravity Waves, Technical Report No. 3, University of Chicago, Department of the Geophysical Sciences, August, 1969.

Meadows, G.A., "Time Dependent Fluctuations in Longshore Currents," Proceedings of the Fifteenth Conference on Coastal Engineering, pp. 660-680, ASCE, 1976.

Miller, R.L., and Ziegler, J.M., "The Internal Velocity Field in Breaking Waves," Proceedings of the Ninth Conference on Coastal Engineering, pp. 103-122, ASCE, 1964.

Steer, R., Kinematics of Water Particle Motion within the Surf Zone, M.S. Thesis, Naval Postgraduate School, Monterey, California, 1972.

Thornton, E.B., "A Field Investigation of Sand Transport in the Surf Zone," Proceedings of the Eleventh Conference on Coastal Engineering, pp. 335-351, ASCE, 1968.

Thornton, E.B., and Krapohl, R. F., "Water Particle Velocities Measured under Ocean Waves," Journal of Geophysical Research, v. 79, pp. 847-852, 20 February 1974.

Thornton, E.B., and Richardson, D. P., The Kinematics of Water Particle Velocities of Breaking Waves within the Surf Zone, Technical Report NPS-58T 74011A, Naval Postgraduate School, Monterey, California, January 1974.

Thornton, E.B., "Review of Status of Energetics and Momentum Fluxes in the Surf Zone: Field Data," Proceedings of the Workshop on Coastal Sediment Transport Processes, University of Delaware, 2-4 December 1976.

Thornton, E.B., Galvin, J.J., Bub, F.L. and Richardson,D.P., "Kinematics of Breaking Waves within the Surf Zone," Proceedings of the Fifteenth Conference on Coastal Engineering, pp. 461-476, ASCE, 1976.

Walker, J.R., Estimation of Ocean Wave-Induced Particle Velocities from the Time History of a Bottom Mounted Pressure Transducer, M.S. Thesis, University of Hawaii, 1969.

INITIAL DISTRIBUTION LIST

		No. Copies
1.	Defense Documentation Center Cameron Station Alexandria, Virginia 22314	2
2.	Library, Code 0142 Naval Postgraduate School Monterey, California 93940	2
3.	Department Chairman, Code 68 Department of Oceanography Naval Postgraduate School Monterey, California 93940	3
4.	Associate Professor E. B. Thornton, Code 68Tm Department of Oceanography Naval Postgraduate School Monterey, California 93940	5
5.	LT A. J. Olsen 5806 N. 19th St. Arlington, Virginia 22205	3
6.	Oceanographer of the Navy Hoffman Building No. 2 200 Stovall Street Alexandria, Virginia 22332	1
7.	Office of Naval Research Code 410 NORDA NSTL, Station, MS 39529	1
8.	Dr. Robert E. Stevenson Scientific Liaison Office, ONR Scripps Institution of Oceanography La Jolla, CA 92037	1
9.	Library, Code 3330 Naval Oceanographic Office Washington, D.C. 20373	1
10.	SIO Library University of California, San Diego P. O. Box 2367 La Jolla, CA 92037	1
11.	Department of Oceanography Library University of Washington Seattle, WA 98105	1

12. Department of Oceanography Library — 1
    Oregon State University
    Corvallis, Oregon 97331

13. Director — 1
    Naval Oceanography and Meteorology
    National Space Technology Laboratories
    NSTL Station, MS 39529

14. NORDA — 1
    NSTL Station, MS 39529

15. Commanding Officer — 1
    Fleet Numerical Weather Central
    Monterey, CA 93940

16. Commanding Officer — 1
    Naval Environmental Prediction Research Facility
    Monterey, CA 93940

17. Department of the Navy — 1
    Commander Oceanographic System Pacific
    Box 1390
    FPO San Francisco 96610

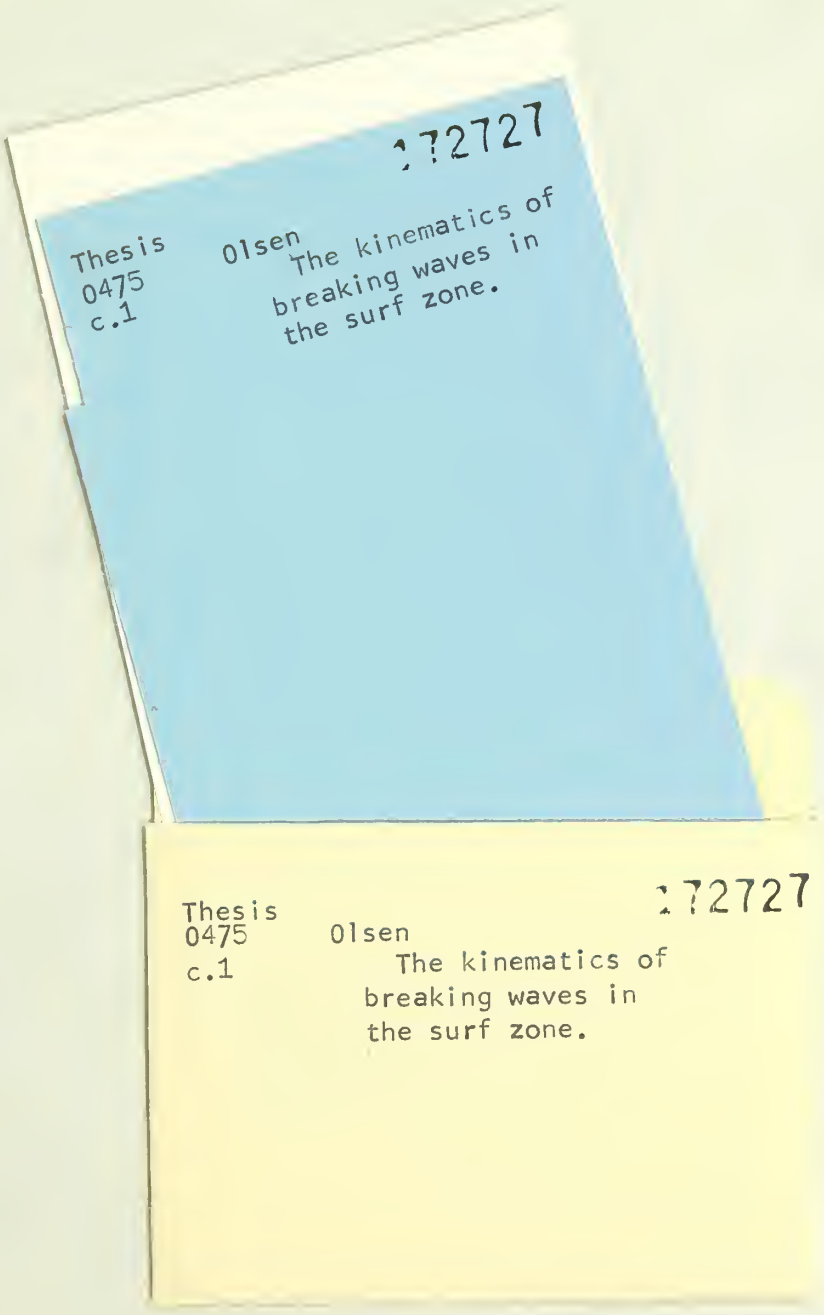

Thesis
0475
c.1

172727

Olsen
The kinematics of
breaking waves in
the surf zone.